Earth and Environmental Science Transactions of the Royal Society of Edinburgh, **100**, 15–33, 2010 (for 2009)

The sanukitoid series: magmatism at the Archaean–Proterozoic transition

Hervé Martin[1a,b,c], Jean-François Moyen[2] and Robert Rapp[3]

[1a] Clermont Université, Université Blaise Pascal, Laboratoire Magmas et Volcans, BP 10448, F-63000 Clermont-Ferrand, France

[1b] CNRS, UMR 6524, LMV, F-63038 Clermont-Ferrand, France

[1c] IRD, R 163, LMV, F-63038 Clermont-Ferrand, France
Email: h.martin@opgc.univ-bpclermont.fr

[2] Department of Geology, University of Stellenbosch, Private Bag X 01, 7602 Matieland, South Africa

[3] Research School of Earth Sciences, The Australian National University, Canberra, ACT, 0200 Australia

ABSTRACT: A specific type of granitoid, referred to as sanukitoid (Shirey & Hanson 1984), was emplaced mainly across the Archaean–Proterozoic transition. The major and trace element composition of sanukitoids is intermediate between typical Archaean TTG and modern arc granitoids. However, among sanukitoids, two groups can be distinguished on the basis of the Ti content of the less differentiated rocks of the suite: high- and low-Ti sanukitoids. Melting experiments and petrogenetic modelling show that they may have formed by either (1) melting of mantle peridotite previously metasomatised by felsic melts of TTG composition, or (2) by reaction between TTG melts and mantle peridotite (assimilation). Rocks of the sanukitoid suite were emplaced at the Archaean–Proterozoic boundary, possibly marking the time when TTG-dominated granitoid magmatism changed to a more modern-style, arc-dominated magmatism. Consequently, the intermediate character of sanukitoids is not only compositional but chronological. The succession of granitoid magmatism with time is integrated in a plate tectonic model where it is linked to the thermal evolution of subduction zones, reflecting the progressive cooling of Earth: (1) the Archaean Earth's heat production was high enough to allow the production of large amounts of TTG granitoids formed by partial melting of recycled basaltic crust ('slab melting'); (2) at the end of the Archaean, due to the progressive cooling of the Earth, the extent of slab melting was reduced, resulting in lower melt:rock ratios. In such conditions the slab melts can be strongly contaminated by assimilation of mantle peridotite, thus giving rise to low-Ti sanukitoids. It is also possible that the slab melts were totally consumed in reactions with mantle peridotite, subsequent melting of this 'melt-metasomatised mantle' producing the high-Ti sanukitoid magmas; (3) after 2·5 Ga, Earth heat production was too low to allow slab melting, except in relatively rare geodynamic circumstances, and most modern arc magmas are produced by melting of the mantle wedge peridotite metasomatised by fluids from dehydration of the subducted slab. Of course, such changes did not take place exactly at the same time all over the world. The Archaean mechanisms coexisted with new processes over a relatively long time period, even if they were subordinate to the more modern processes.

KEY WORDS: geochemistry, granitoid, magma/melt interactions, petrogenesis, slab melting, temporal change in magma production

The genesis of the continental crust started very early in Earth's history: indeed, detrital zircons from Jack Hills, in Western Australia record the existence of 4·40 Ga granitic (*s.l.*) crust (Wilde *et al.* 2001). Whilst the first half of Earth history mainly corresponds to the extraction of juvenile crust from the mantle, recycling mechanisms existed before 4·0 Ga ago (Cavosie *et al.* 2004, 2005, 2006; Watson & Harrison 2005; Harrison & Schmitt 2007; Blichert-Toft & Albarède 2008), but were highly subordinated processes. Due to the greater Earth heat production (Brown 1985), the petrogenetic processes that operated were different from modern ones, resulting in the genesis of unique lithologies such as komatiites and massive volumes of tonalite trondhjemite and granodiorite (TTG) magmas (Viljoen & Viljoen 1969; Glikson 1971; Windley & Bridgwater 1971; Arth & Hanson 1972; Barker & Arth 1976; McGregor 1979; Condie 1981; Jahn *et al.* 1981; Martin *et al.* 1983). Based on petrological and experimental studies, as well as on geochemical modelling, the genesis of Archaean TTG has been explained by partial melting of hydrous basalt metamorphosed into garnet-bearing amphibolite or eclogite (Barker & Arth 1976; Martin 1986, 1987, 1993, 1994; Rapp *et al.* 1991, 2003; Rapp & Watson 1995; Martin *et al.* 1997, 2005; Foley *et al.* 2002; Martin & Moyen 2002). In contrast, it is more seldom proposed that TTG are generated by the extensive fractional crystallisation of water-rich basalt in a subduction environment (Kamber *et al.* 2002; Kleinhanns *et al.* 2003). If most researchers consider that TTG were generated by the melting of hydrated basalt, they disagree about the exact site where this melting took place. The two end-member possibilities are: (1) partial melting of basalt which underplated

 doi:10.1017/S1755691009016120

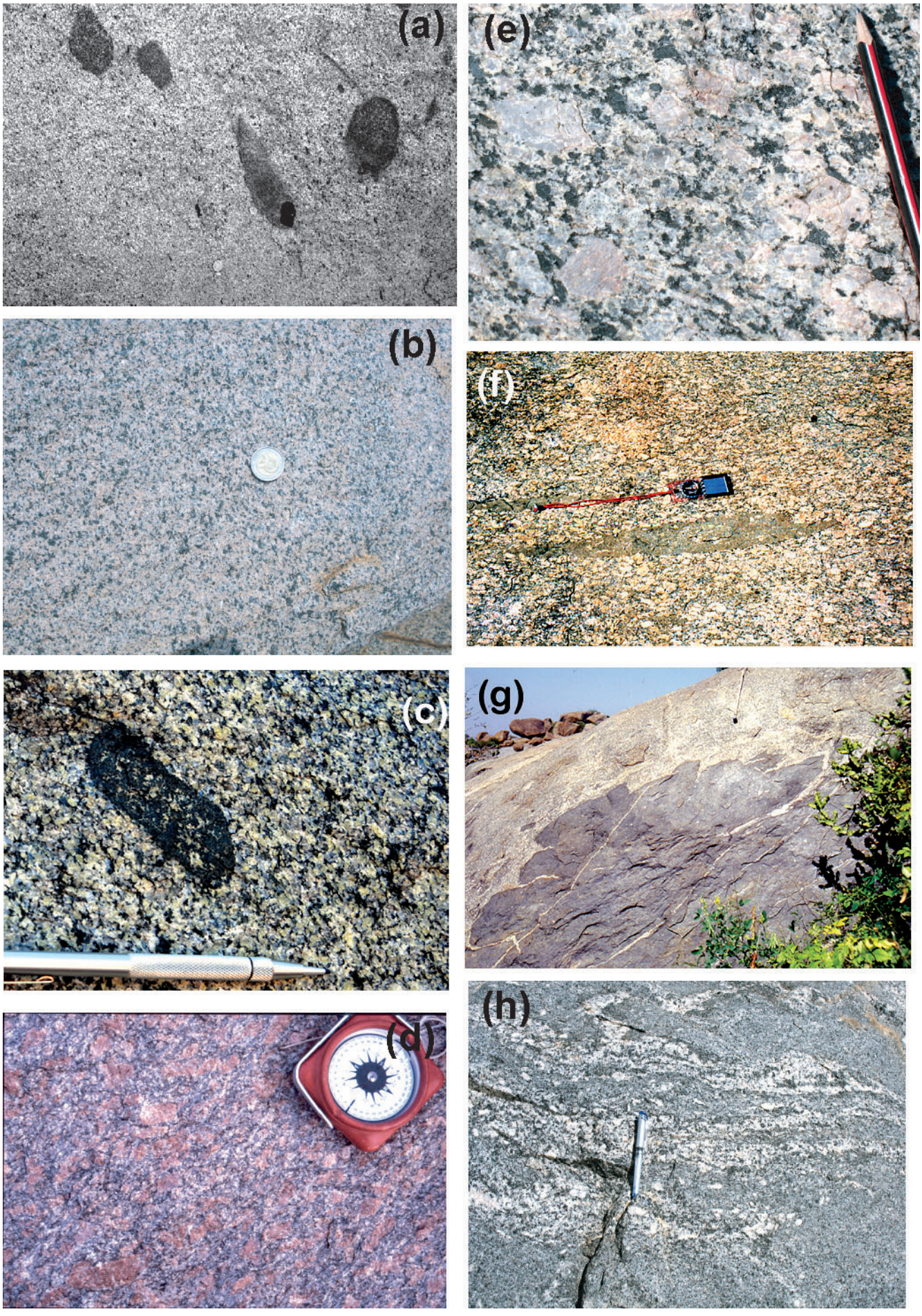

https://doi.org/10.1017/S1755691009016120 Published online by Cambridge University Press

a thickened crust (Atherton & Petford 1993; Rudnick 1995; Albarède 1998; de Wit 1998; Smithies 2000; Smithies *et al*. 2005; Bédard 2006); (2) a subducted hot oceanic slab that melted rather than dehydrating (Martin 1986; Condie 1989; Rollinson 1997; Barth *et al*. 2002; Foley *et al*. 2002; Kamber *et al*. 2002; Martin & Moyen 2002; Rapp *et al*. 2003; Condie 2005; Nair & Chacko 2005; Martin *et al*. 2008). After the end of the Archaean (2·5 Ga), and until today, most of the juvenile continental crust is formed by melting of a fluid metasomatised peridotite followed by different degrees of differentiation, generating the BADR (Basalt Andesite Dacite Rhyolite) suites typical of subduction environments. There, the source of the magmas is considered as being the mantle wedge peridotite metasomatised by fluids resulting from the dehydration of the subducted slab (Tatsumi 1989; Pawley & Holloway 1993; Liu *et al*. 1996; Schmidt & Poli 1998; Forneris & Holloway 2003).

The transition between TTGs and BADRs roughly took place at the Archaean–Proterozoic transition, about 2·5 Ga ago. At the same period, high-Mg dioritic, tonalitic and granodioritic magmatic rocks were generated and emplaced into all Archaean cratons. These plutons, commonly called late granodioritic or granitic plutons, were first identified by Shirey & Hanson (1984), who referred to them as Archaean sanukitoids. These rocks are now found in most Late Archaean terranes (2·9–2·5 Ga) (Shirey & Hanson 1984; Stern 1989; Stern & Hanson 1991; Smithies & Champion 1999; Moyen *et al*. 2001b, 2003); they possess both modern (classical calc-alkaline differentiation, similar to BADR association, high transition element contents) and Archaean (low HREE contents, strongly fractionated REE patterns, etc. . . .) geochemical characteristics. The transitional character of sanukitoids is not only compositional but also chronologic, being emplaced during the 'hinge' period between two epochs dominated by TTG (Archaean) and BADR (Proterozoic/Phanerozoic) juvenile crustal magmatism. Consequently, their study could provide not only new insights into the change in petrogenetic mechanisms during this period, but also into the changing geodynamics on Earth across the ∼2·5 Ga boundary.

The purpose of this paper is: (1) to review the geochemical and petrologic characteristics of sanukitoids; (2) to address their petrogenesis; (3) to discuss possible geodynamic environments for their generation; and (4) to consider their temporal distribution over the whole of Earth's crustal evolution.

1. Sanukitoids

1.1. Definition

Shirey & Hanson (1984) first recognised a suite of Late Archaean felsic intrusive and volcanic rocks in the Superior Province that had both mineralogical and chemical characteristics clearly different from TTG, which had up until then been viewed as, volumetrically, the overwhelmingly dominant granitoid throughout the Archaean. Because the major element geochemistry of these rocks resembled that of Miocene high-Mg Andesite (Sanukite) from the Setouchi volcanic belt of Japan (e.g. Tatsumi & Ishizaka 1982), Shirey & Hanson (1984) referred to them as 'Archaean sanukitoids'. Since this pioneering work, sanukitoids have been described in most Archaean terranes: the Superior Province (Shirey & Hanson 1984, 1986; Stern & Hanson 1991; Bédard 1996; Stevenson *et al*. 1999), Wyoming (Frost *et al*. 1998), the Baltic shield (Querré 1985; Lobach-Zhuchenko *et al*. 2000, 2005, 2008; Halla 2005; Kovalenko *et al*. 2005; Samsonov *et al*. 2005; Käpyaho 2006), South India (Balakrishnan & Rajamani 1987; Jayananda *et al*. 1995; Krogstad *et al*. 1995; Moyen *et al*. 2001b, 2003; Sarvothaman 2001), China (Jahn *et al*. 1998), Limpopo (Barton *et al*. 1992; Millonig *et al*. 2008), the Central Pilbara craton (Smithies & Champion 1999) and the Amazonian craton (Medeiros & Dall'Agnol 1988; Althoff 1996; Leite *et al*. 2004). Compared with TTG, sanukitoids still represent a volumetrically subordinate component of the Archaean crust; however, they are a common component of most Late Archaean cratons.

1.2. Composition

Based on field observations, sanukitoids define a complete magmatic series, from diorites to granites (the 'sanukitoid suite' of Stern & Hanson 1991). The two most common rock types are: (1) medium-grained, equigranular monzodiorites to granodiorites, containing small (5–10 mm) clusters of biotite, hornblende and rare relicts of hornblende-rimmed clinopyroxene, which give the rock a very distinctive, black and white 'spotted' aspect; (Fig. 1a–b); (2) porphyritic monzogranite (Fig. 1d–e), with large (2–5 cm) to very large (∼10 cm) phenocrysts of K-feldspar in a coarse-grained matrix.

In both case, the paragenesis consists of quartz, plagioclase ($An_{20–30}$), perthitic microcline, hornblende and biotite. Accessory phases are magnetite, ilmenite, epidote, sphene, apatite, zircon and allanite. Microgranular, mafic dioritic to monzodioritic enclaves are common (Fig. 1c, f–h); they are fine grained (0·1–1 mm), with occasional K-feldspar phenocrysts with rapakivi texture. They also typically contain small mafic clusters of biotite with 'spots' of dull black amphibole. In some places, relict diopside has been observed within amphibole grains.

Sanukitoid can occur as plutons of all sizes, with a broad range of crustal emplacement levels and degrees of heterogeneity. For example, sanukitoids in the Central Pilbara Craton (Smithies & Champion 1999) form small (<1 km), homogeneous stocks of shallowly emplaced magmas, whereas sanukitoids of South India (the 'Closepet granite', Jayananda *et al*. 1995; Moyen *et al*. 1997, 2001a), form a huge intrusive body that is about 400 km long and 20 km wide and is rooted in the lower granulitic crust. The porphyritic monzogranite of the Closepet batholith is associated with migmatites and anatectic granites derived from melting of the surrounding TTG basement.

Sanukitoid compositions range between mafic (SiO_2 ∼ 50% and MgO ∼ 8%) and felsic (SiO_2 ∼ 75% and MgO ∼ 0·1%) end-members (Fig. 2). This could result either from differentiation of a primitive parental magma (e.g. Reddy 1991; Stern & Hanson 1991) or from contamination by older crustal

Figure 1 Field appearance of sanukitoids: (a)–(c) medium-grained, equigranular monzodiorite (Low-Ti sanukitoid); (d)–(h), porphyritic monzogranite (High-Ti sanukitoid). (a) Typical sanukitoid amphibole granodiorite; 2·55 Ga 'Dod gneisses', Kolar belt, India (Krogstad *et al*. 1991; Chardon *et al*. 2002). (b) Biotite ± amphibole bearing granodiorite in the 2·67 Ga Matok Pluton, Limpopo Belt, South Africa (Kreissig *et al*. 2001). (c) Mafic microgranular enclave-bearing sanukitoid of the Rio Maria terrane, Amazonian Craton, Brazil (courtesy R. Dall'Agnol) (Medeiros & Dall'Agnol, 1988). (d) Porphyritic monzogranite from the Closepet batholith, South India. (e) Porphyritic monzogranite in the 2·57 Ga Bulai Pluton, Limpopo Belt, South Africa (Barton *et al*. 1992). (f). Stretched microgranular mafic enclave in the Closepet batholith. (g) Pillowed (monzo-) dioritic enclave, Closepet. (h) Mingling relationships between a porphyritic monzogranite and monzodiorites, Matok.

https://doi.org/10.1017/S1755691009016120 Published online by Cambridge University Press

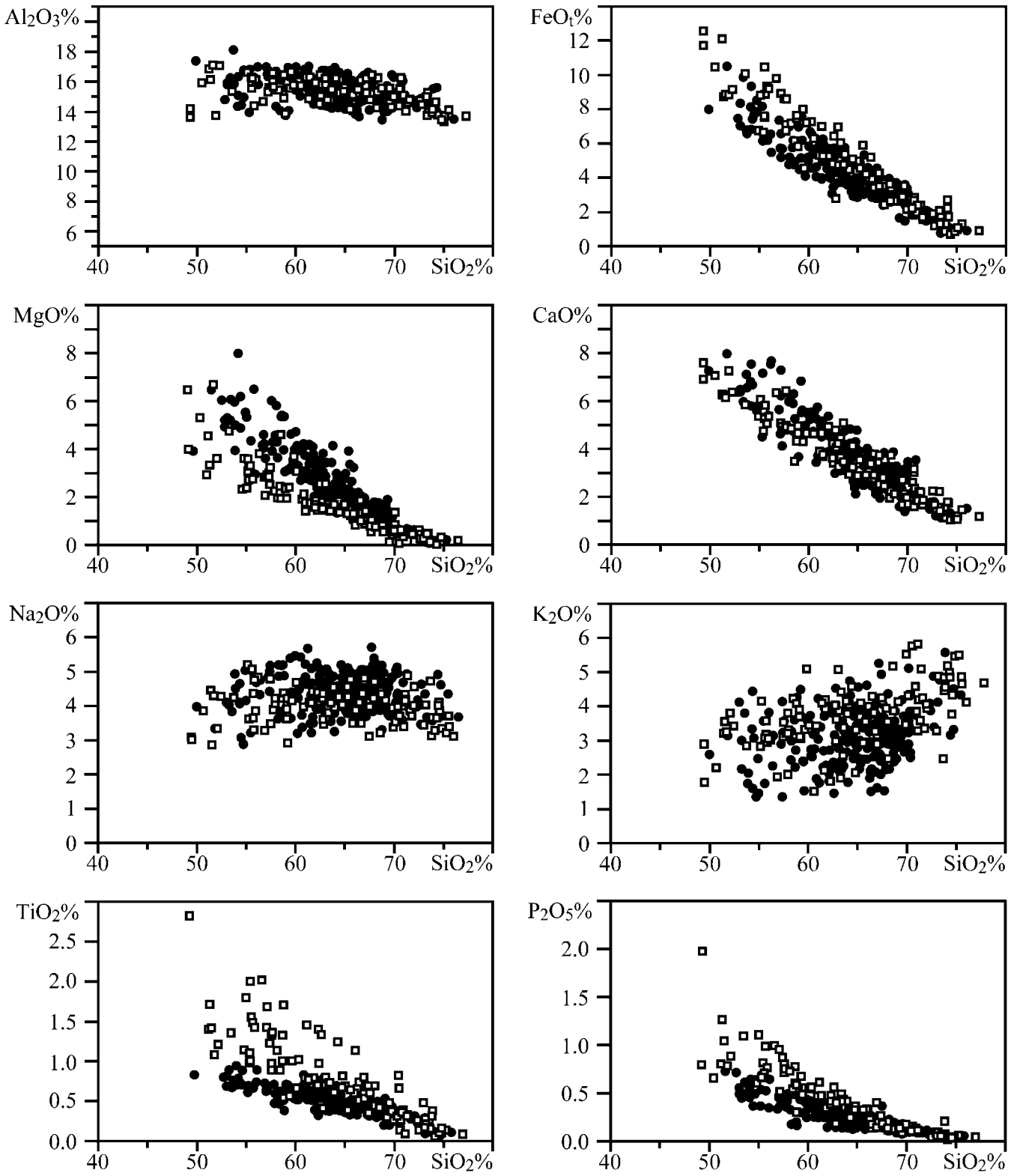

Figure 2 Harker diagrams for both low-Ti (filled circles) and high-Ti (open squares) sanukitoids.

components during emplacement (Moyen *et al*. 2001a). For the Closepet batholith for example, it has been demonstrated (Jayananda *et al*. 1995; Moyen *et al*. 1997, 2001a; among others) that the linear trends for both major and trace elements, over a wide variation of SiO_2 contents (from ~50% up to 75%) are the result of crustal contamination. In this case, mantle-derived magmas interacted with the crust in which they intruded. Their mantle characters were obliterated and altered by a superimposed crustal signature, such that they were often considered to have a mixed origin.

The details of this 'late' evolution are not the focus of this paper, which deals with the origin of the juvenile component, regardless of its subsequent evolution. Consequently, this paper will only refer to the less differentiated component of the sanukitoid suites, thus excluding all samples with SiO_2>62%, that are assumed to be strongly modified by either interaction with a felsic crustal component, or by differentiation of these primary magmas.

The differences between the two main petrologic types identified above (medium-grained, equigranular monzodiorites

https://doi.org/10.1017/S1755691009016120 Published online by Cambridge University Press

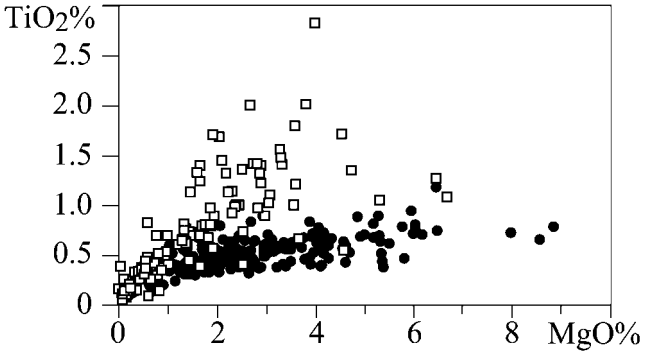

Figure 3 TiO_2 *vs.* MgO plot showing that for the same degree of differentiation (anti-correlated with MgO), TiO_2 content is significantly higher in porphyritic monzogranite (open squares) than in medium-grained, equigranular monzodiorites (filled circles), thus supporting the discrimination between two groups of sanukitoids (Low-Ti and high Ti).

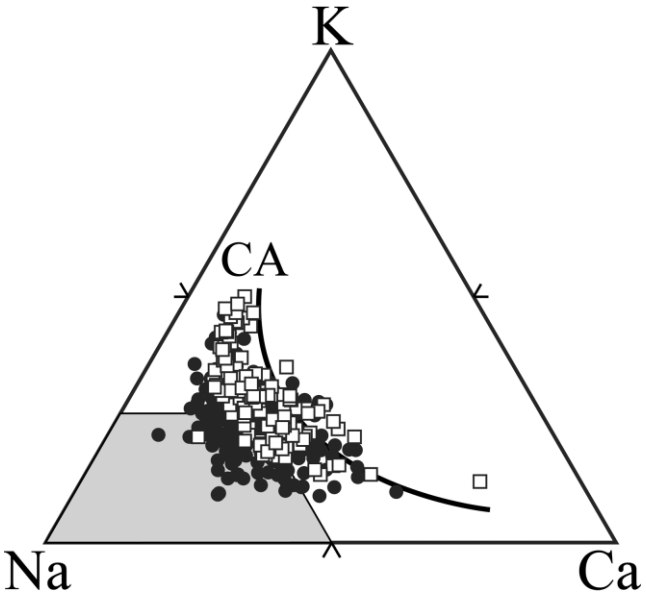

Figure 4 Cationic Ca–Na–K diagram showing that both the low-Ti (filled circles) and high-Ti (open squares) sanukitoids are different of Archaean TTG (grey field, Martin *et al.* 2005). They show a K-enrichment, thus occupying a position intermediate between TTG and the classical calc-alkaline trend (CA) as defined by Barker & Arth (1976). It must also be noted that the high-Ti sanukitoids are slightly K-richer than the low-Ti ones.

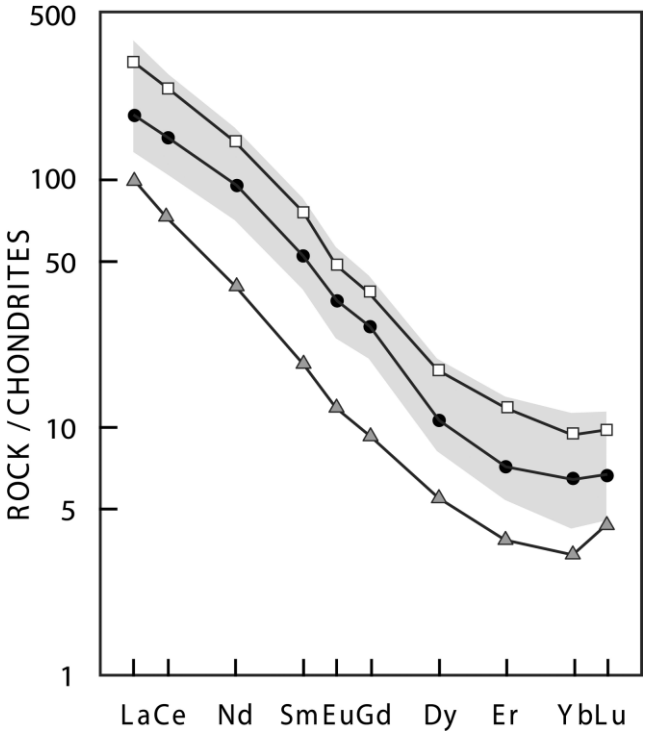

Figure 5 Chondrite normalised REE patterns for average Archaean TTG (grey triangles), low-Ti (filled circles) and high-Ti (open squares) sanukitoids with SiO_2<62%. The grey field represents the compositional field for sanukitoids. Normalisation values are from Masuda *et al.* (1973) divided by 1·2.

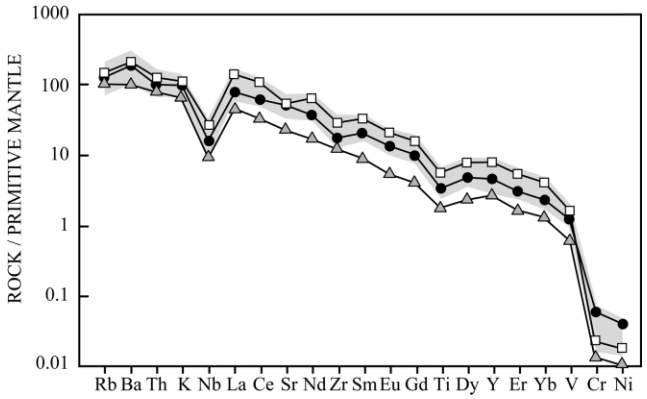

Figure 6 Primitive mantle (Sun & McDonough 1989) normalised multi element diagram for average Archaean TTG (grey triangles), both low-Ti (filled circles) and high-Ti (open squares) sanukitoids with SiO_2<62%. The grey field represents the compositional field for sanukitoids.

and porphyritic monzogranite), are not only textural, but also correspond to geochemical differences. Figure 2 shows that for some elements (e.g., Al_2O_3, Na_2O and K_2O), chemical trends are exactly the same in the two groups, but for other elements the geochemical evolution differs, particularly for the less differentiated rocks. This is well exemplified by the TiO_2 *vs.* SiO_2 (Fig. 2) or TiO_2 *vs.* MgO (Fig. 3) plots, where for the same degree of differentiation, TiO_2 content is significantly higher in porphyritic monzogranite than in medium-grained, equigranular monzodiorites. Consequently, it is proposed to discriminate these two sanukitoid types on the basis of their TiO_2 content: in this paper, the medium-grained, equigranular monzodiorites will subsequently be referred to as low-Ti sanukitoids, whereas the porphyritic monzogranites will be referred as high-Ti sanukitoids.

In a K–Na–Ca cationic triangle (Fig. 4), sanukitoids do not show any affinity with Archaean TTG (Martin *et al.* 2005) and rather show an evolution trend similar to the classical calc-alkaline differentiation trend of Barker & Arth (1976). It must be noted that the low-Ti sanukitoids are slightly poorer in K and richer in Na than their high-Ti equivalents.

Table 1 reports the average composition of 104 sanukitoids from the literature. Out of the published data, only samples with SiO_2 lower than 62% were kept, as they are considered to be representative of the mafic pole of the differentiation suites – regardless of the differentiation mechanism involved. These 104 analyses were classified into 57 low-Ti- and 47 high-Ti sanukitoids, whose average composition is also given. The sanukitoids are meta-aluminous (A/CNK = 0·79) and moderately potassic (K_2O/Na_2O = 0·72). Mg# (molecular Fe/(Fe + Mg)) is quite high (0·53), as are Ni and Cr contents (54 and 104 ppm, respectively). Sr and Ba are typically greater than 1000 ppm (1108 and 1471 ppm respectively); Na_2O (4·31%) and K_2O (3·11%), (as well as most LILE) contents are also high. Similarly, LREE (e.g. La_N = 234) contents are high

https://doi.org/10.1017/S1755691009016120 Published online by Cambridge University Press

Table 1 Average composition and standard deviation for 104 sanukitoids from the literature. Only samples with SiO_2 lower than 62% were taken into consideration, as they are considered as representative of the mafic pole of the differentiation suites, regardless of the differentiation mechanism that operated. These 104 analyses fall into two groups: 57 are low-Ti- and 47 are high-Ti sanukitoids. The average compositions of 250 modern arc granitoids (Martin 1994) and 1094 TTGs (Martin *et al.* 2005) are also given for comparison. Fe_2O_3*=Total iron expressed as Fe_2O_3; Mg#=molecular ratio Mg/(Mg+Fe); A/CNK=molecular ratio Al/(Ca+Na+K).

	TTG (*n=1094*)		Sanukitoid <62% SiO_2 (*n=104*)		Low-Ti Sanukitoid <62% SiO_2 (*n=57*)		High-Ti Sanukitoid <62% SiO_2 (*n=47*)		Modern Arc Granitoids (*n=250*)	
	Average	*Std. dev.*	Average	*Std. dev.*	Average	*Std. dev.*	Average	*Std. dev.*	Average	*Std. dev*
wt.%										
SiO_2	69·51	*3·64*	58·65	*3·56*	59·18	*3·31*	58·00	*3·47*	68·1	*6·2*
Al_2O_3	15·59	*1·14*	16·14	*1·10*	16·08	*1·07*	16·22	*1·39*	15·07	*1·6*
Fe_2O_3*	3·24	*1·56*	6·75	*1·94*	6·14	*1·49*	7·50	*1·71*	4·36	*2*
MnO	0·05	*0·05*	0·12	*0·07*	0·10	*0·03*	0·13	*0·07*	0·09	*0·1*
MgO	1·25	*0·77*	3·90	*1·41*	4·33	*1·27*	3·39	*1·83*	1·55	*1*
CaO	3·16	*1·11*	5·53	*1·24*	5·52	*1·33*	5·55	*1·39*	3·06	*0·64*
Na_2O	4·72	*0·77*	4·31	*0·73*	4·49	*0·75*	4·09	*0·82*	3·68	*0·49*
K_2O	1·95	*0·77*	3·11	*0·82*	3·04	*0·85*	3·20	*0·88*	3·4	*1·1*
TiO_2	0·38	*0·21*	0·93	*0·42*	0·69	*0·18*	1·21	*0·46*	0·54	*0·32*
P_2O_5	0·15	*0·10*	0·56	*0·27*	0·42	*0·12*	0·72	*0·31*	0·15	*0·08*
ppm										
Rb	66	*43*	87	*43*	83	*37*	92	*38*	110	*50*
Ba	713	*465*	1471	*601*	1493	*575*	1445	*699*	715	*205*
Nb	7	*5*	13	*7*	10	*3*	17	*7*	12·1	*5*
Sr	490	*217*	1108	*512*	1202	*563*	994	*366*	316	*150*
Zr	135	*108*	237	*112*	172	*55*	316	*104*	171	*53*
Y	12	*16*	27	*14*	20	*7*	35	*13*	26	*5*
Th	7	*0·6*	9	*7*	9	*5*	10	*9*	11·8	*6·5*
Ni	18	*17*	54	*33*	69	*28*	36	*41*	10·5	*8*
Cr	40	*75*	104	*73*	143	*60*	58	*55*	23	*15*
V	48	*29*	118	*43*	110	*34*	127	*42*	76	*45*
La	31·4	*23·8*	73·9	*42·2*	57·0	*17·4*	94·4	*51·6*	31	*9*
Ce	57·8	*257·0*	152·4	*66·7*	120·5	*34·0*	191·1	*90·7*	67	*17*
Nd	22·4	*17·0*	69·7	*28·1*	56·5	*16·0*	85·8	*37·4*	27	*7*
Sm	4	*2·3*	11·7	*4·7*	9·5	*2·8*	14·3	*5·9*	5·3	*14*
Eu	0·9	*0·4*	2·8	*1·1*	2·4	*0·7*	3·3	*1·2*	1	*0·5*
Gd	2·4	*1·4*	7·8	*2·9*	6·7	*2·0*	9·2	*2·4*	5·5	*1*
Dy	1·7	*0·9*	4·4	*1·8*	3·5	*1·2*	5·5	*1·2*	5·2	*0·1*
Er	0·76	*0·49*	1·97	*0·88*	1·49	*0·55*	2·56	*0·68*	3	*1*
Yb	0·64	*0·40*	1·60	*0·78*	1·29	*0·50*	1·98	*0·76*	3·2	*0·5*
Lu	0·13	*0·50*	0·26	*0·12*	0·21	*0·07*	0·32	*0·11*	0·5	*0·1*
K_2O/Na_2O	0·41		0·72		0·68		0·78		0·92	
Mg#	0·43		0·53		0·58		0·47		0·41	
A/CNK	1·00		0·79		0·78		0·80		0·98	
$(La/Yb)_N$	32·4		30·5		29·2		31·5		6·4	

and HREE (e.g. Yb_N=7·7) moderately low, resulting in strongly fractionated patterns ($(La/Yb)_N$=30·5); which do not show any significant Eu anomaly (Fig. 5). In addition, high-Ti sanukitoids are enriched in REE relative to their low-Ti counterparts. On a primitive mantle-normalised multi-element diagram (Fig. 6), sanukitoids (both types) do not show significant negative anomalies in Zr or Y and only a small negative one for Ti.

On Harker plots, (Fig. 2), both low and high-Ti sanukitoids plot on a single trend for most elements (Al_2O_3, CaO, Na_2O, K_2O and partly FeO_t), pointing to the fact that the two groups formed from a similar source by similar mechanisms. Only MgO and TiO_2 depict slightly different trends that converge towards a common silica-rich pole. This confirms that the differences between the two groups do not reflect differentiation mechanisms, but rather correspond to distinct mafic end-members. Figures 5 and 6 also show that both REE and multi-element patterns are parallel, except for a slight negative Sr anomaly in high-Ti sanukitoids that does not exist in the low-Ti group. This parallelism strongly militates in favour of a similar source for the two facies. In addition, the trace element patterns are also essentially parallel to those of average Archaean TTG, leading us to conclude that TTG are genetically related to sanukitoids in some way.

1.3. Petrogenesis

The average Mg# in sanukitoids is 0·53, but can reach values >0·65 in the more mafic samples. These very high Mg#s and correspondingly high Cr and Ni concentrations (>100 ppm and >300 ppm respectively) in the most primitive members of the sanukitoid suites preclude a crustal (including basaltic) source; for reference, the Mg# of experimental TTG liquids

https://doi.org/10.1017/S1755691009016120 Published online by Cambridge University Press

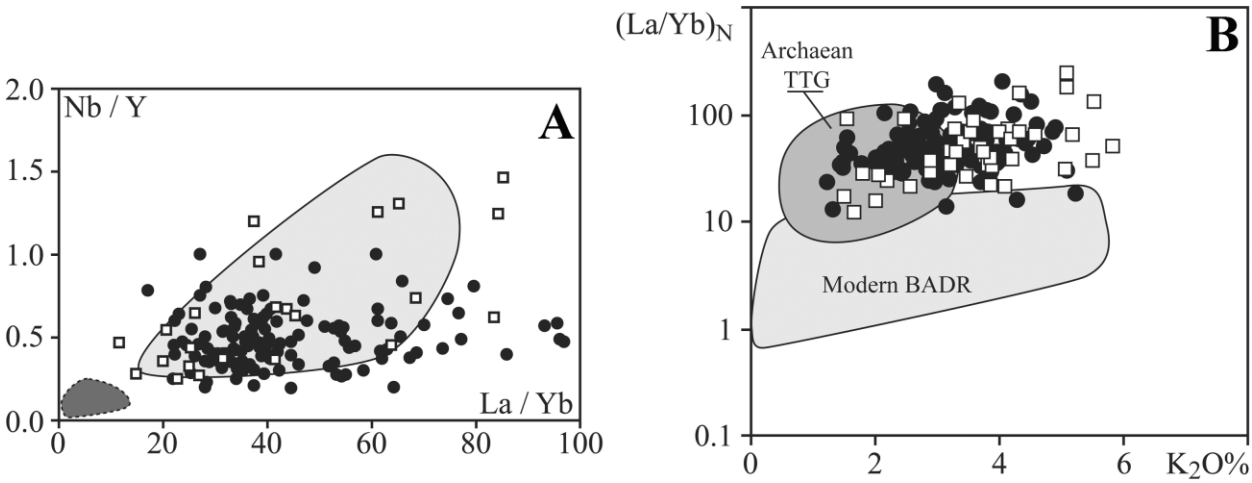

Figure 7 (A) (Nb/Y) *vs.* (La/Yb) plot for low-Ti (filled circles) and high-Ti (open squares) sanukitoids with SiO_2<62%. The dark grey field is that of arc magmas generated by melting of a peridotite metasomatised by fluids. Data are from Fiji (Rogers & Setterfield, 1994) and the New Hebrides (Monzier *et al.* 1997). The light grey field is that of modern high-Mg andesites considered to be generated by the melting of a mantle peridotite enriched by felsic melts. Data are from Baja California (Calmus *et al.* 2003) and Ecuador (Bourdon *et al.* 2003; Hoffer 2008). See text for more detailed explanation. Sanukitoids point to a mantle source metasomatised by felsic melts. (B) $(La/Yb)_N$ *vs.* K_2O plot that compares the composition of sanukitoids with that of typical arc BADR suites (Martin 1994). Sanukitoids, draw a trend parallel to that of BADR field, thus pointing to similar petrogenetic mechanisms and source. However, the fact that the field of Archaean TTG perfectly plots on one extremity of the sanukitoid trend indicates the possible role of a metasomatic agent played by TTG magma.

generated by partial melting of basalts never exceeds 0·45 (Rapp & Watson 1995; Zamora 2000). Similarly the SiO_2 content of the less differentiated TTG is of about 60% (Martin 1994), whereas it is of about 50% in sanukitoids. Therefore, the source of sanukitoids must be ultramafic. On the other hand, the same rocks are very rich in LILE; which because of the high Mg#, Cr and Ni, precludes any interpretation in terms of enrichment through fractional crystallisation, as this process would efficiently deplete compatible elements from the magmas (Martin & Sigmarsson 2007). Contamination of an LILE-rich felsic continental crust by komatiitic or basaltic magmas could also generate sanukitoid magmas. However, Stern (1989), and more recently Smithies & Champion (1999) modelled the interaction between mafic (or ultramafic) melts and the felsic crust, and demonstrated that this process cannot reproduce both characteristics of primitive sanukitoids (high Mg#, Ni and Cr together with high SiO_2 and LILE contents). Therefore, the present authors interpret the LILE enrichment as a primary characteristic, reflecting the nature of the source; that source must at least in part be ultramafic (because of the high Mg#s, Cr and Ni), and LILE enriched; the only reliable and realistic possibility is that sanukitoids derive from a source formed by the interaction of a felsic (TTG) melt and ultramafic rock (mantle peridotite). The sanukitoid melt itself may come about from a single stage process of melt infiltration, hybridisation, and assimilation (e.g., Rapp *et al.* 1999), or in a two-stage process in which melt metasomatism is followed by partial melting of the metasomatised peridotitic source.

In a modern subduction zone, where a metasomatised and geochemically enriched mantle wedge is the main source of arc magmatism, two metasomatic agents, (both derived from crustal components of the subducting oceanic lithosphere) are generally invoked: hydrous, solute-rich, possibly supercritical fluids, and hydrous, SiO_2-rich (i.e., felsic) melts. These two metasomatic agents have very contrasted behaviour with respect to some chemical elements like HFSE; for instance $Kd_{Nb}^{solid/fluid}$ >10, whereas $Kd_{Nb}^{solid/melt}$ <1. In other words, hydrous fluids are unable to transfer Nb from the slab into the mantle wedge, whereas a felsic melt can. In addition, felsic melts generated within the garnet stability field will have an 'adakitic' signature characterised by very low Y and Yb contents (Martin *et al.* 2005; Macpherson *et al.* 2006; Moyen 2009). Consequently, the nature of the metasomatic agent can be discussed in the (Nb/Y) *vs.* (La/Yb) diagram (Fig. 7A), where the composition of sanukitoids is compared with that of modern arc magmas. The dark grey field is that of modern magmas from New Hebrides (Monzier *et al.* 1997) and Fiji (Rogers & Setterfield 1994) where the magmatic signature is free of any continental contamination and where the metasomatic agent is considered to be exclusively fluids produced by sub-solidus dehydration of the subducted slab. The light grey field is that of modern high-Mg andesites and low-silica adakites (Bourdon *et al.* 2003; Hoffer 2008), which are also considered to be the result of partial melting of melt-metasomatised mantle peridotite. Since Late Archaean sanukitoids have higher Nb/Y and La/Yb than typical modern arc magmas, a fluid-metasomatised mantle source can be ruled out. On the other hand, sanukitoids overlap the field for high-Mg andesites or low-silica adakites, magmas that are considered as generated either through partial of a mantle peridotite metasomatised by adakitic melts (Martin *et al.* 2005, for review), or by direct reaction (assimilation) of mantle peridotite with TTG melts (e.g., Rapp *et al.* 1999). In addition, Figures 5 and 6 shows that except for transition elements, the REE and multi-element patterns of sanukitoids are strictly parallel to TTG patterns, thus pointing to a strong genetic link between them. This conclusion is reinforced by the $(La/Yb)_N$ *vs.* K_2O plot (Fig. 7B), comparing the composition of sanukitoids with typical arc BADR suites and Archaean TTGs (Martin 1994). Sanukitoids follow a trend parallel to the BADR field, with the same range of K_2O contents, $(La/Yb)_N$ being closely correlated with K_2O. This reflects the similarity of the petrogenetic processes: possibly melting of a metasomatised mantle. However, the BADR and sanukitoid trends are parallel but not superimposed, the later having higher $(La/Yb)_N$, indicating different metasomatic agents; the overlap between the TTG field and the end of the sanukitoid trend points to TTGs being a possible metasomatic agent.

https://doi.org/10.1017/S1755691009016120 Published online by Cambridge University Press

Collectively, these evidences show that the most likely metasomatic agent responsible for the peridotitic source enrichment is a TTG-like felsic melt.

2. Experimental petrology

The only way to obtain appreciable volumes of LILE-enriched magmas from a peridotitic source is by enrichment of the mantle source prior to melting. This would imply a two-stage petrogenetic process for sanukitoid magmas in which melting is preceded by metasomatism, i.e., the reaction between an LILE-enriched fluid or melt and mantle peridotite. As discussed above (Fig. 7), this metasomatic agent is considered as being an SiO_2-rich melt. In a modern subduction zone setting, these felsic melts are presumed to be produced by partial melting of subducted basaltic oceanic crust, referred to as 'adakites', a term more or less synonymous with the 'slab melt' (henceforth referred to as 'pristine' adakites, to denote a slab melt that has yet to experience modification by reaction with mantle peridotite). As Archaean TTG, the chemistry of adakites shows that they are derived by partial melting of garnet-bearing mafic (metabasaltic) crust, followed by variable degrees of subsequent 'interaction' with mantle peridotite, presumably in the overlying mantle wedge (see Martin *et al.* 2005, for review). Given the geochemical evidence presented above for a genetic link between TTG granitoids and sanukitoids, a number of experimental studies looking at various aspects of chemical interaction between TTG liquids and peridotite have been undertaken in recent years (e.g. Sen & Dunn 1994; Yaxley & Green 1998; Rapp *et al.* 1999, 2006; Prouteau *et al.* 2001; Hoffer 2008). These studies focused on the equilibrium between the 'hybridised slab melt' (Rapp *et al.* 1999) and the modified peridotite assemblage. They implicitly assume a 'one-stage' process, in which the adakitic (or TTG) melt is transformed into a sanukitoid on its way up to the surface; sanukitoid forms contemporaneously with the geological event that generated the felsic melt (Fig. 8).

Earlier experimental studies in the 1970s and 1980s examined processes of 'melt hybridisation in subduction zones' (Nicholls & Ringwood 1973; Sekine & Wyllie 1982; Johnson & Wyllie 1989), where 'assimilation of mantle peridotite by an ascending slab-derived melt' led to the formation of 'zones of hybrid olivine pyroxenite which, in turn, could be remelted to generate a spectrum of island arc magmas' (Nicholls & Ringwood 1973; Johnson & Wyllie 1989). This scenario immediately calls to mind a 'two-stage' process, in which the metasomatic event is separated in time from the melting (or remelting) event, which yields sanukitoids (Fig. 8).

Deciding between a 'one-stage' and a 'two-stage' process is difficult, if not impossible, on experimental grounds alone. Indeed, the only conclusions that can be drawn from experiments is that a sanukitoid melt can be formed in equilibrium with a mafic to ultramafic mineral assemblage, which provides no constrains on the path that was followed in the P–T–X space to reach these conditions, let alone the duration of this path.

A critical factor in the reaction between slab-derived, pristine melts and peridotite in the mantle wedge is the so-called 'effective melt-to-rock ratio' (Rapp *et al.* 1999), which refers to the relative proportions of adakite melt and peridotite 'rock' involved in the 'melt-rock reaction' (Kelemen *et al.* 1993, 1998). This parameter is obviously easily controlled in laboratory experiments, but in nature, it depends upon the scale at which the interaction between slab-derived melts and the mantle wedge are considered, as well as the physical mechanism for melt infiltration (e.g., porous flow? fracture propagation?). The melt:rock ratio can be high; this does not mean that the mantle as a whole was soaked with melts, but rather that the scale of the interactions was such that only limited portions of the mantle were allowed to react with the melt. In other words, low melt:rock ratios correspond to interactions involving large amounts of the mantle – maybe corresponding to narrow magma pathways, or magma percolating through the mantle on a grain-scale, with a correspondingly high interface surface between melt and mantle. In contrast, high melt:rock ratios can be obtained where large magma conduits restrict the contact surface between the melt and the peridotite, and/or high magma flow in large conduits reduces the time range available for interaction, and/or armouring of the edges of the conduit makes further reactions difficult or impossible. Consequently, in natural geological systems, the melt:rock ratio can vary between zero and infinity, as a function of the magma flow rate, overall supply, and of the size and geometry of the magma pathways, and the mechanism involved in melt infiltration and transport.

Regardless of these issues, melt–rock reactions in the overlying mantle wedge above a subducting slab can generally be assumed to be dominated by processes of assimilation when the effective melt:rock ratio is high (one-stage process; Fig. 8), and by cryptic and modal metasomatic processes when the effective melt:rock ratio is low. In the former case, mantle-hybridised adakitic melts will be produced, and in the latter case a melt-metasomatised peridotite (*sensu lato*) mantle wedge is formed, which itself can then become the source for magmas by subsequent partial melting events (i.e., the 'two-stage' process; Fig. 8).

The composition of 'mantle-hybridised slab melts' and the metasomatic mineral assemblages that form as a result of such melt–rock reactions in the mantle wedge, will clearly depend upon such factors as the 'effective melt:rock ratio', pressure, temperature, and water content (all strictly controlled in laboratory experiments), and comprehensive and systematic experimental studies are lacking. Nevertheless, certain general observations can be made regarding the processes of peridotite assimilation, melt hybridisation, and mantle metasomatic reactions from the laboratory experiments that have been carried out. First, olivine is consumed in these reactions (i.e., reactant phases are olivine and pristine adakite melt), and the primary metasomatic phases are orthopyroxene and amphibole or phlogopite (i.e., products). Secondly, at high melt:rock ratios and/or relatively high temperatures, most, if not all, of the original olivine in the peridotite is consumed, and one is left with a hybridised adakitic melt in equilibrium with a pyroxenite reaction residue (Rapp *et al.* 1999; Prouteau *et al.* 2001). At low melt:rock ratios and/or lower temperatures, the metasomatic phase assemblage is dominated by amphibole/phlogopite and orthopyroxene, and although generally some of the original olivine is also present, it is often not clear from the experiments whether or not 'armouring' of the original olivine by orthopyroxene has taken place (Sen & Dunn 1994; Rapp *et al.* 1999; Prouteau *et al.* 2001), In this case the trace element signature of the slab melt is effectively transferred to the mantle wedge, and this adakite-metasomatised pyroxenite then becomes a potential source for 'mantle-derived' melts in the future. Martin *et al.* (2005) have classified the melts that are associated with these two different outcomes of slab melt-peridotite reactions in the mantle wedge as 'high-SiO_2 adakites' (HSA; mantle-hybridised adakites), and 'low-SiO_2 adakites' (LSA; partial melts of adakite-metasomatised peridotite). It is important to note that, although the experimental analogues of 'HSAs' have been produced in the laboratory (e.g., Rapp *et al.* 1999), experimental 'LSAs' have not. The

https://doi.org/10.1017/S1755691009016120 Published online by Cambridge University Press

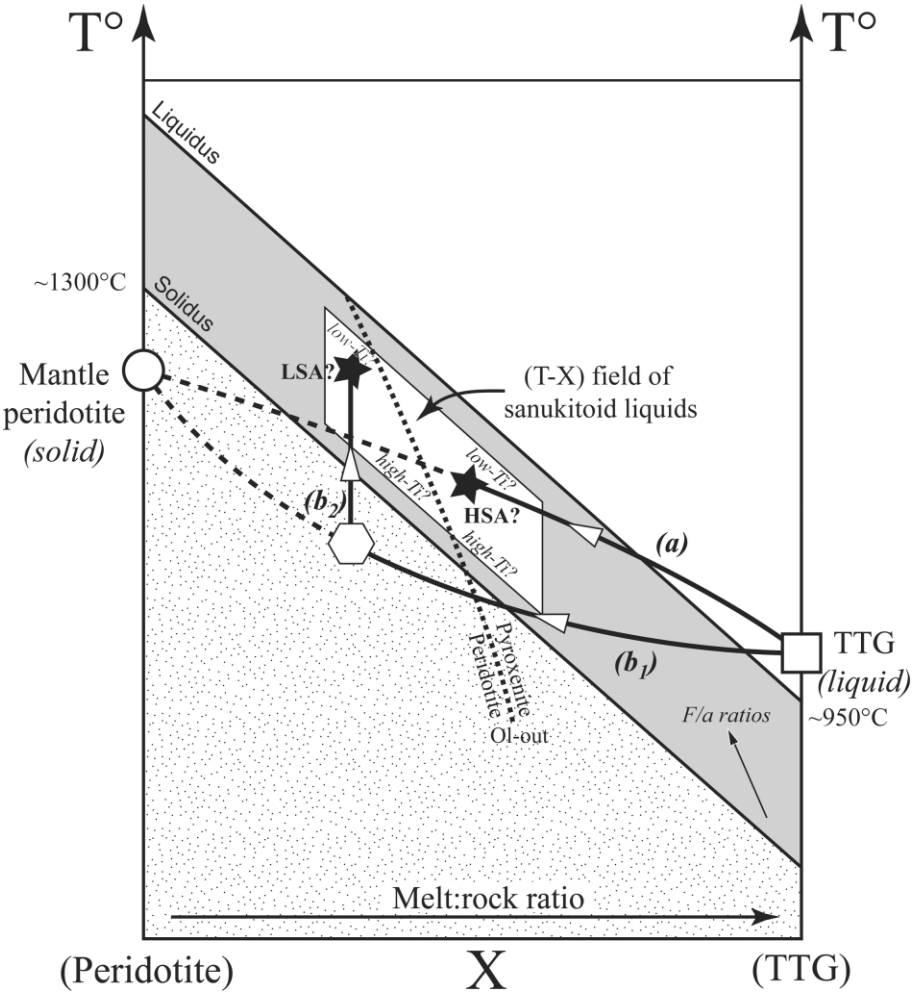

Figure 8 Schematic diagram summarising the possible modes of interactions between TTG liquids and mantle wedge peridotites. This diagram reports the temperature (T°) *vs.* the bulk composition of the system (X). X ranges between a pure peridotite and a pure TTG liquid. In a 'true' pseudosection, both the liquidus and solidus curves would probably be stepped; however for purpose of simplification, they are drawn as lines. The dotted line represents the (conceptual) limit of stability for olivine, i.e. the limit between peridotitic and pyroxenitic solids (residuum if in equilibrium with the melt, 'metasomatised mantle' otherwise). Sanukitoid liquids exist for bulk compositions that are mixtures of TTG and peridotite, and for melt fractions ranging between the solidus and the liquidus (white parallelogram field). This field can be reached along different paths. Path (*a*) is the 'one-stage' process mentioned in the text. In this case the TTG liquid reacts with peridotites to give a sanukitoid liquid in equilibrium with a mafic or ultramafic solid. HSA liquids probably form along this trend (for high melt:rock ratios); lower TTG proportions would rather result in LSA or sanukitoids. Path (*b*) is the 'two-stage' process, (b_1) is the complete assimilation of TTG liquids via metasomatic reactions with the peridotite, and (b_2) corresponds to subsequent melting of this modified composition. The black *F/a* arrow shows how the *F/a* ratio (discussed in section 3) increases, inside the inter solidus–liquidus domain.

present authors expect that in fact a petrogenetic and compositional continuum probably exists between HSA and LSA magmas, and where a given magma falls along that continuum is probably highly dependent upon the mechanism and dynamics of melt infiltration and propagation.

The distinction between the two groups (HSAs and LSAs) may in fact lie in the nature of the mineral assemblage with which they may have equilibrated: experimental results have shown that HSA melts are in equilibrium with a pyroxenite residue ($\pm$ garnet $\pm$ amphibole/phlogopite), whereas LSA melts are likely to be in equilibrium with an olivine-bearing (i.e., peridotite or garnet peridotite) phase assemblage, with the melting reaction being controlled by the breakdown of metasomatic amphibole and/or phlogopite. Hirose (1997) does report partial melts of hydrous lherzolite at 1·0 GPa that have the appropriate major-element composition of LSAs (e.g., SiO_2 = 54–60 wt.%), and are in equilibrium with a spinel peridotite residue (ol + opx $\pm$ cpx + spl). Unfortunately, in this paper no trace element data was available. In the present interpretation of LSA and sanukitoid petrogenesis, the peridotitic source in these experiments would have experienced a metasomatism event prior to melting, in order for the TTG or 'slab melt' signature to be transferred to the mantle. The Late-Archaean sanukitoids are equated (Fig. 9) with LSA melts, possibly in equilibrium with an olivine-bearing pyroxenitic residue.

3. Discussion

3.1. Numerical modelling of sanukitoid genesis and diversity

The chemical composition of sanukitoid liquids obtained by experimental fusion can be reproduced using numerical modelling, which provides important clues in understanding the details of petrogenetic mechanisms. For instance, it allows the processes that lead to the difference between low- and high-Ti

https://doi.org/10.1017/S1755691009016120 Published online by Cambridge University Press

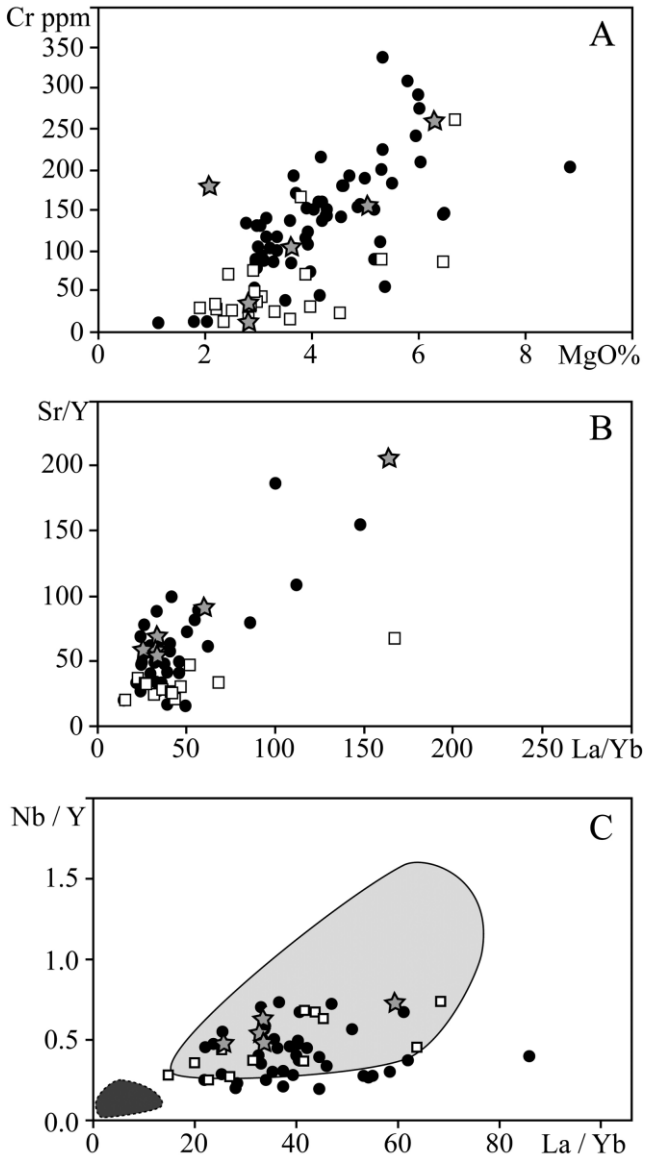

Figure 9 Diagrams comparing the composition of low-Ti (filled circles) and high-Ti (open squares) sanukitoids with SiO_2<62%, with liquids experimentally produced by interaction between a mantle peridotite and an Archaean TTG melt (grey stars) (Rapp *et al.* 2006): (A) Cr *vs.* MgO; (B) Sr/Y *vs.* La/Yb; (C) Nb/Y *vs.* La/Yb. Experimental melts display compositions identical with sanukitoids; in addition, inset (C) also shows that all experimental liquids plot in the light grey field, which is the field of modern high-Mg andesites considered as generated by melting of a mantle peridotite enriched by felsic melts (see Fig. 7 and text for more details).

sanukitoids to be addressed. Both types share many characteristics (Figs 2–6). However, systematic differences are observed for a few key geochemical parameters (mostly compatible elements ratios), as summarised in section 1.2, where it has been demonstrated that they reflect different, albeit related, primitive magmas. These differences could be accounted for by two distinct processes: (1) different degree of melting of a same source; and (2) different degrees of metasomatism of a mantle peridotite by TTG melts. A simple model has been built (Moyen 2009) in order to take into account the co-variations of these two parameters; it mimics the experimental procedure and is simply based on the batch melting of a mantle peridotite, which composition has been modified by mixing with TTG melt. If the concentration of an element in the mantle before metasomatism is C_m, it becomes C_{mm} after metasomatism by a mass fraction a of TTG melt; C_{TTG} being the concentration of the element in the TTG melt. C_{mm} is given by the mixing equation (1)

$$C_{mm}=a.C_{TTG}+(1-a).C_m \text{ (Equation 1)}$$

The melt:rock ratio in the sense of Rapp *et al.* (1999, 2006), i.e. the relative melt and rock proportions actually involved in the interactions, is represented by $a/1-a$.

The composition of the melt (C_l) is given by the equilibrium melting equation (Shaw 1970) where F is the degree of melting and D the general distribution coefficient:

$$C_l = \frac{C_{mm}}{F + D(1-F)} \text{ (Equation 2)}$$

Partition coefficients are from Rollinson (1993). For Fe and Mg, 'pseudo' partition coefficients were calculated from minerals phases found in adakite-metasomatised peridotite nodules (Kepezhinskas *et al.* 1996; Grégoire *et al.* 2008). Equilibrium melting is used to ensure consistency with experimental results, which are by construction at (or near) equilibrium. While simple, this model nevertheless allows for melt consumption ($a>F$) or, conversely, additions to the melt ($F>a$) during the interactions; the parameter F/a indicates the amount of melt gained or lost during the interactions. The difficulty consists in assigning realistic values for a and F, thus leading to a poorly constrained model. However, it appears that the only relevant parameter controlling the composition of the melt after the interaction with peridotite is the F/a ratio (Moyen 2009), i.e. the net gain or loss of melt during the process (Fig. 10). With increasing F/a values (i.e., towards a net melt gain – the interactions result in more addition to the melt than formation of new minerals by reactions between the melt and the peridotite), the resulting melt evolves to higher Mg#, but also lower incompatible element contents (REE, Sr, Y), and lower La/Yb and Sr/Y ratios. In contrast, low F/a values (i.e., the interactions result mostly in the formation of new minerals out of the melt, reducing its net volume) concentrate the incompatible elements, increase the La/Yb and Sr/Y ratios, and generate lower Mg# melts – although still with values higher than in the non-reacted TTG. In the same way as experimental petrology, this model is based on equilibrium between liquid and mineral phases for a given bulk composition X (P and T are implicit in the choice of mineral phases used for the calculation of D); consequently, the model cannot *per se* provide constrains on the P–T path (i.e., a one- or two-stage process) followed to reach the final P–T–X state.

The FeO, MgO and TiO_2 behaviour is adequately accounted for by this model (Fig. 11). Indeed, decreasing F/a ratios result in a diminution of MgO correlated with a slight increase in FeO and a significant augmentation of TiO_2, thus adequately providing an explanation for the difference between low- and high-Ti sanukitoids. However, some of the high-Ti sanukitoids display TiO_2 contents that are too high to be accounted by the present model. This can be explained by the choice of some parameters in the calculation: average TTG compositions (TiO_2=0·38%) were used as a 'starting material', but TTG compositions are actually more diverse, and TiO_2 contents of 0·7–0·8% are not rare. Such a TiO_2-richer TTG melt would easily account for the high-Ti sanukitoid characteristics. An alternative possibility is that the basic hypothesis of this model – equilibrium melting – is not true. Indeed, in the case of selective melting of only the Ti-rich portion of the metasomatised mantle (i.e., the amphibole-rich portion), without allowing bulk equilibrium with the residuum, the resulting liquid can be Ti-enriched well over that predicted by equilibrium models.

https://doi.org/10.1017/S1755691009016120 Published online by Cambridge University Press

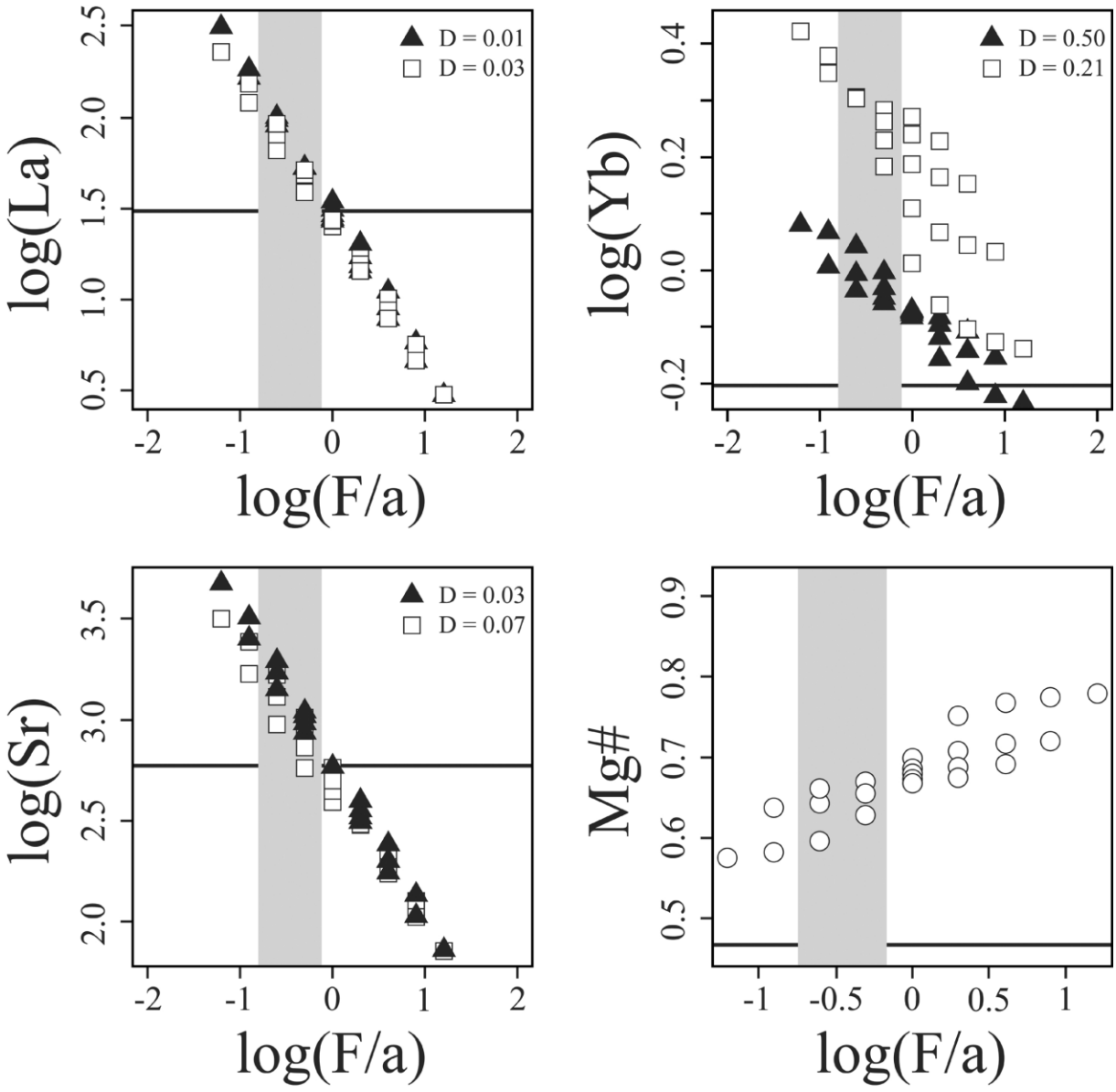

Figure 10 Log(La), log(Yb), log(Sr) and Mg# *vs*. Log(F/a). *F* represents the proportion of liquid (degree of melting) and *a* the degree of metasomatism of a peridotitic source by TTG melts. The light grey domain corresponds to the *F/a* ratios that yield values closer to those measured in sanukitoids. Triangles and squares respectively represent the presence and absence of garnet during melting of the mantle peridotite. The thick black horizontal line corresponds to the average TTG composition used in the model. The D values used in computation are also given (see text and Moyen 2009 for more details).

Therefore, it is proposed that the difference between the high- and the low-Ti series essentially reflects differences in the *F/a* ratio (Fig. 8): the high-Ti group formed by low F/a (low degree of melting and/or more enriched source), and melting was probably far from equilibrium, allowing amphibole breakdown to control the melt's composition without re-equilibrating with the rest of the rock. In contrast, the low-Ti group could correspond to higher (*F/a*) (high degree of melting and/or lower source enrichment), in conditions close to equilibrium melting. These two situations may reflect different geological/geodynamical scenarios; indeed, whereas the low-Ti situation can arise in one single event, in which the mantle contamination and the generation of the sanukitoid melt are concomitant, the disequilibrium scenario envisioned for the high-Ti group requires a two-step process, in which amphibole is allowed to physically form, before being destroyed by a subsequent selective melting event. This requires a more complex geological history. However, Figure 10 shows that for all elements, the composition of both low- and high-Ti sanukitoids is achieved only for F/a<1, which means that the reaction between TTG melt and mantle is mostly TTG melt consuming leading to the formation of new minerals, in the mantle peridotite. This is consistent with the observed consumption of melt in assimilation experiments between depleted peridotite and 'slab-derived' TTG melts (Rapp *et al*. 1999). Moreover, in the case of a two-stage process, the amount of melt formed is lower than the melt consumed by the initial interactions.

3.2. Residual garnet and conditions of melting

Sanukitoids have an average Yb content of 1·60 ppm, with a correlated high La/Yb=46·2. These values are intermediate between average TTG (Yb=0·64 ppm and La/Yb=59) and typical arc dacites and granodiorites (Yb=4·4 ppm and La/Yb=9·7). Both experimental work (Rapp *et al*. 1999, 2006) and geochemical modelling done on sanukitoids as well as on low-silica adakites (LSA) (Moyen 2009) show that residual garnet is not absolutely necessary to account for the geochemical characteristics of most sanukitoids. The general shape of

https://doi.org/10.1017/S1755691009016120 Published online by Cambridge University Press

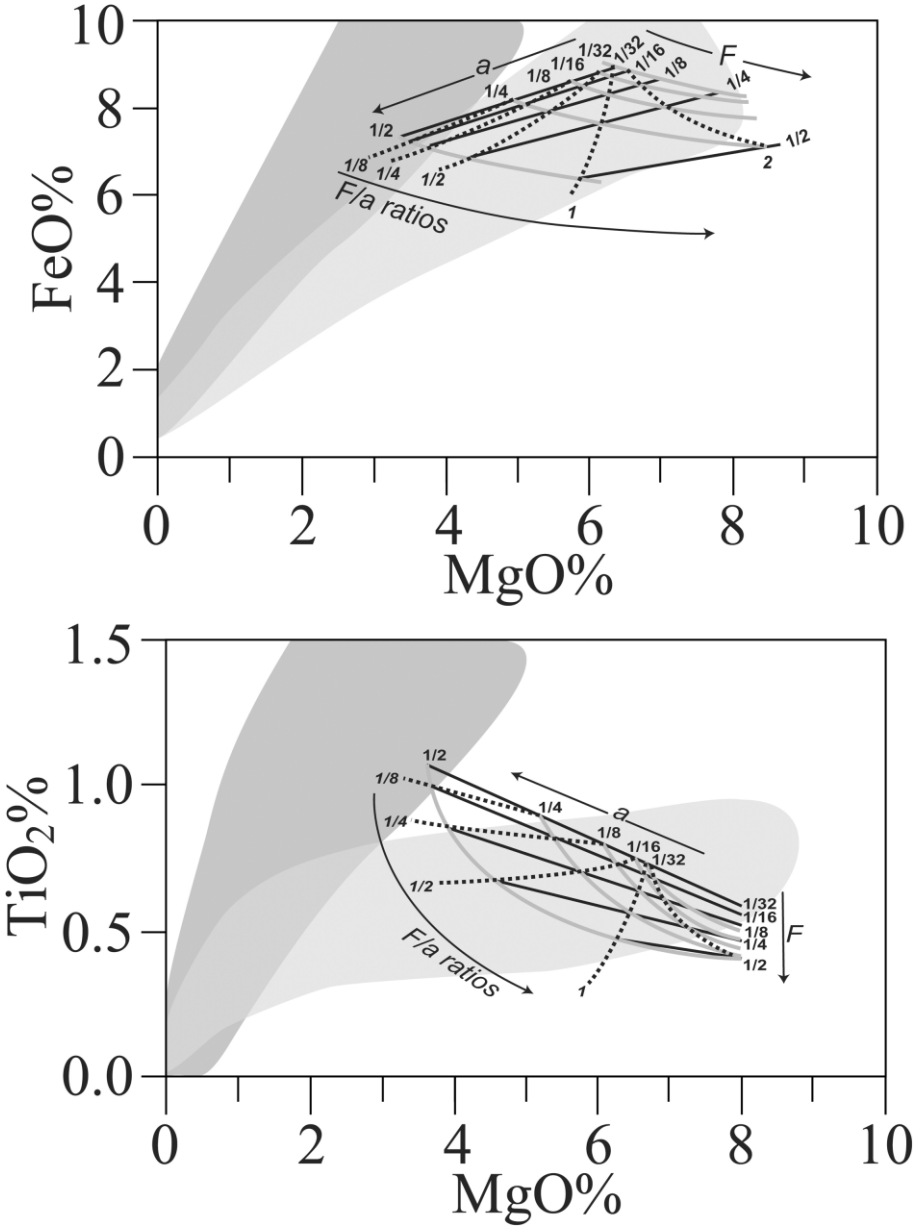

Figure 11 FeO *vs*. MgO and TiO_2 *vs*. MgO diagrams comparing the results of geochemical modelling with the composition of sanukitoids. The dark grey field is that of high-Ti sanukitoids whereas the light grey field represents the low-Ti sanukitoids. In both models, the black and grey lines correspond to the evolution of liquid controlled by *a* and *F* parameters respectively. Dotted lines represent a constant *F*/*a* ratio. These diagrams show a change in the *F*/*a* ratio that accounts for the observed diversity of sanukitoids. (More details are given in the text).

the REE patterns of TTG seems to be transferred to sanukitoids, after a shift to higher values (Yb=0·64 ppm in TTG and 1·6 ppm in sanukitoids). However, experiments and modelling show that the presence of small amounts of residual garnet would make the acquisition of sanukitoid melt characteristics easier. Indeed, Figure 12 is a La *vs*. Yb plot for all sanukitoids; it points to diversity among sanukitoids. The range of La/Yb ratios observed is consistent with the presence of variable proportions of residual garnet during melting. As proposed by Francis & Ludden (1995) and Dalpé & Baker (2000), this garnet could be the result of peritectic reactions associated with the breakdown of amphibole.

The variability in residual garnet could indicate that the TTG melt/mantle peridotite interactions were able to take place over a wide range of pressure, whatever the real mechanism is: direct hybridisation of the TTG melt or remelting of a peridotite metasomatised by TTG melts. It must also be noted that the La/Yb systematic does not coincide with the low/high-Ti classification, thus indicating that the two parameters are independent (both low and high F/a can be realised at shallow as well as at great depths). Garnet stability does not only depend on pressure, but is also controlled by rock composition. In a peridotite, garnet is stable only for pressure higher than 2·5 to 3·0 GPa; whereas for an amphibolitic (basaltic) composition it is stable at pressure as low as 1·0 to 1·2 GPa. Consequently, metasomatism of mantle peridotite by felsic melts will modify the peridotite composition: high TTG input resulting in garnet stable at lower pressure.

Since the density of TTG melts is lower than that of mantle peridotite, they can only ascend through the mantle. This implies that the source for TTG is located below the mantle peridotite. In the case where garnet is stable in the mantle peridotite, this means that TTG melts are necessarily generated at depth greater than 40–60 km, depending on the amount of TTG melt having reacted with mantle peridotite. During melting of amphibolites, the garnet proportion increases with

https://doi.org/10.1017/S1755691009016120 Published online by Cambridge University Press

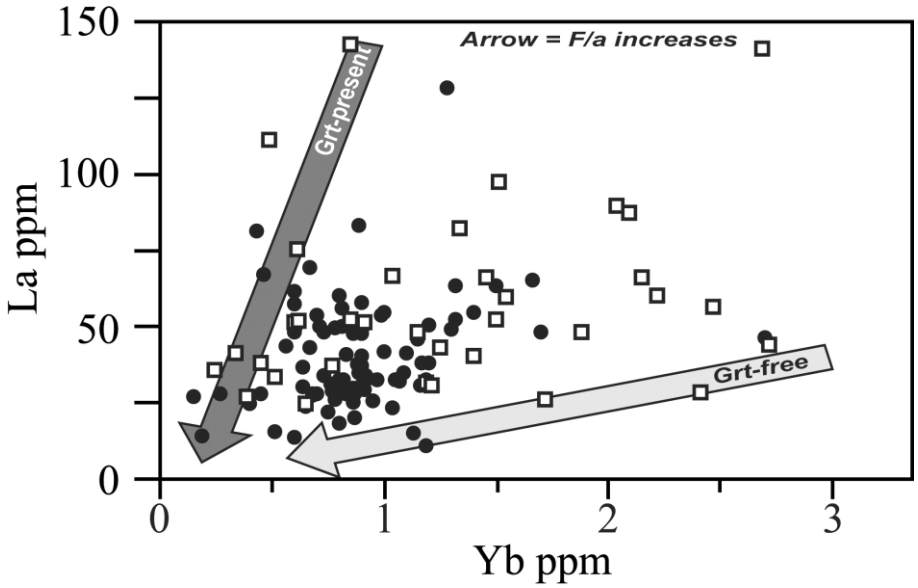

Figure 12 La *vs.* Yb diagram showing the diversity of La/Yb ratios in sanukitoids. La/Yb variations are not correlated with the two-fold low-Ti (filled circles) and high-Ti (open squares) sanukitoid classification. The variability of La/Yb is accounted by different proportions of residual garnet.

depth; in order to have enough garnet to produce a proper TTG composition, the depth of melting must be at least greater than 45–50 km (1·5 GPa) (Moyen & Stevens 2006; Nair & Chacko 2008): which is consistent with the depth of 40–60 km deduced from sanukitoids. This requires a generally efficient geodynamic process able to carry hydrated basalts to depths greater than 40–60km. The only mechanism able to straightforwardly and systematically realise such geometry with hydrous basalts under a mantle slice, at depths of >40–60 km, is subduction. Therefore, sanukitoids can be regarded as markers of at least some kind of subduction, with burial into the mantle of significant portions of surface mafic hydrated material.

3.3. Geodynamic implications and Archaean–Proterozoic boundary

The sanukitoids mainly emplaced at the Archaean–Proterozoic boundary, during a period where the dominant mechanism of genesis of the juvenile continental crust changed from melting of hydrous basalt (Archaean) to fusion of the fluid metasomatised mantle peridotite (post-Archaean). As discussed earlier, evidence supports the genesis of most TTG and sanukitoids in a subduction environment; following this logic, the present authors can propose a general model for the generation of juvenile continental crust across the Archaean–Proterozoic boundary.

Today, the subducted oceanic crust is old (60 Ma on average) and cold; it contributes to the cooling of the mantle wedge, such that geothermal gradient along the Benioff plane is low (Fig. 13) and dehydration reactions in subducted basalt occur before it reaches its hydrous solidus. Consequently, the oceanic slab loses its water and is unable to melt at low temperature. Fluids liberated by dehydration reactions rise up towards the surface through the mantle wedge and induce its partial melting. The rising fluids also transfer soluble elements such as LILE and LREE from the subducted lithosphere into the mantle wedge. In other words, most of the present-day juvenile continental crust is generated in subduction geodynamic environments, by the melting of a mantle wedge, whose composition has been modified by fluids liberated by dehydration of the crustal portions of subducted slabs of oceanic lithosphere. During the Archaean, Earth heat production was greater, resulting in higher geothermal gradients in subduction zones. Along such high geothermal gradients, the order in which the dehydration reaction and hydrous solidus curves are crossed is inverted (Fig. 13): the subducted oceanic slab reaches its hydrous solidus temperature before dehydration begins and is able to melt at relatively low temperature and shallow depth, but deep enough for garnet to be stable in the residue, giving rise to TTG magmas. Consequently, TTG is the result of relatively shallow depth melting of subducted oceanic crust metamorphosed into garnet amphibolite or eclogite. Today, in some exceptional cases, in subduction zones, where an abnormally young oceanic crust is subducted (active ridge subduction such as Patagonia), adakitic magmas are generated; which are very similar to Archaean TTG. This shows that hot geothermal gradients in subduction zones are able to result in slab melting and TTG-like magma genesis (see Martin 1999; Smithies 2000; Martin *et al.* 2005, for discussion and overviews).

Recently, Smithies (2000), Smithies & Champion (2000) and Martin & Moyen (2002), showed that the chemical composition of the parental magma of TTG has changed through Archaean times. These authors consider that change as progressive, whereas Condie (2005) sees it as an abrupt event at about 2·7 Ga. According to Martin & Moyen (2002), the Mg# of the more primitive TTG magmas increased from maximum values of 0·45 at 4·0 Ga to 0·65 at 2·5 Ga. In the same period, the maximum concentrations of Ni and Cr increased, as Sr did, from ~550 ppm at 3·8 Ga to ~1200 ppm at 2·5 Ga (Fig. 14). On the other hand, the high Mg# (0·65) of the younger TTG (<3·0 Ga), is higher than values determined by experimental high-pressure melting of basaltic material, which requires that a mantle component played a role in the genesis of these magmas. Consequently, this time-related change is interpreted in terms of a secular increase of the interactions between the TTG parental and the mantle wedge peridotites (e.g. Maury *et al.* 1996; Rapp *et al.* 1999; Smithies 2000; Martin & Moyen 2002). Similarly, these authors interpret the Sr content in TTG parental magmas in terms of plagioclase stability; indeed, not only Sr content increases in course of time, but also ($CaO+Na_2O$) and Al_2O_3. As plagioclase stability is pressure dependent; they conclude that, from 4·0 Ga to 2·5 Ga the depth of melting of the subducted slab progressively increased.

https://doi.org/10.1017/S1755691009016120 Published online by Cambridge University Press

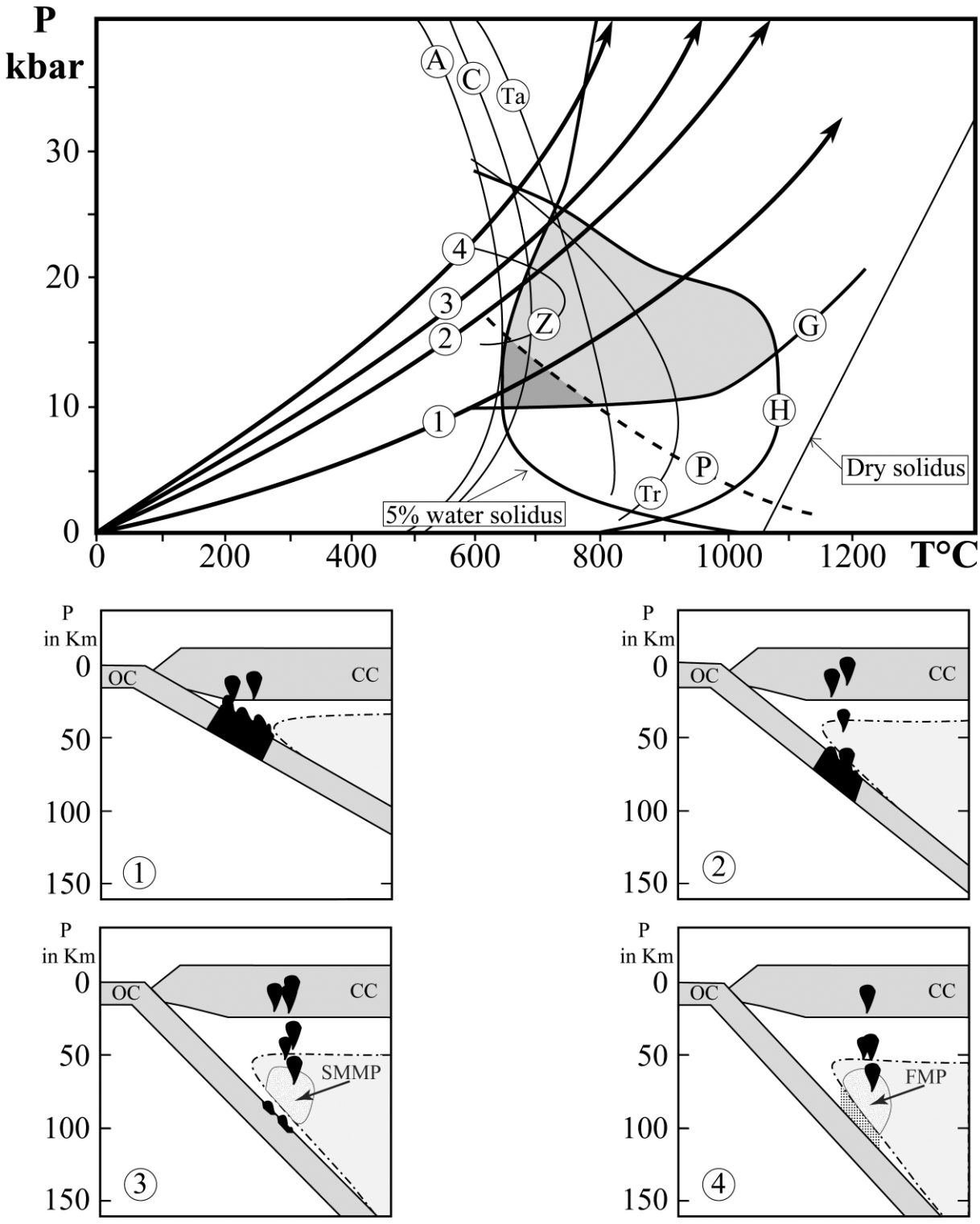

Figure 13 P–T diagram and synthetic cross-sections of subduction zones (after Martin & Moyen 2002). (1) In the Early Archaean (4·0 Ga) the geothermal gradient along the Benioff plane was very high, thus the subducted slab melts at shallow depth. Due to the thinness of the wedge and the low temperature, mantle and melt interactions are limited or absent; (2) After 3·0 Ga, the Earth was cooler, the geothermal gradient was lower and slab melting occurred at greater depth. The overlying mantle wedge is thick and hot, and interactions can occur between mantle and slab melts; (3) At the Archaean–Proterozoic transition, geothermal gradients are too low to allow a high degree of slab melting. Slab melts are almost totally consumed in a reaction with the mantle. Low-Ti sanukitoid are assumed to be the result of a single event of contamination of slab melts by peridotite, whereas low-Ti sanukitoids formed through a two-step process where the mantle metasomatised by slab melts is subsequently molten; (4) After 2·5 Ga, geothermal gradients are so low that slab melting is precluded. The oceanic crust dehydrates and the liberated fluids metasomatise the mantle wedge, whose melting produces modern arc magmatism. Dehydration reactions: H=hornblende out; A=antigorite out; C=chlorite out; Ta=talc out; Tr=tremolite out; Z=zoisite out. G and P lines represent stability fields of garnet and plagioclase respectively. Grey field is P–T TTG window. OC=oceanic crust; CC=continental crust; dotted line=solidus of hydrous mantle; black areas=magma; dotted area=fluids; SMMP=slab melt metasomatised peridotite; FMP=fluid metasomatised peridotite.

https://doi.org/10.1017/S1755691009016120 Published online by Cambridge University Press

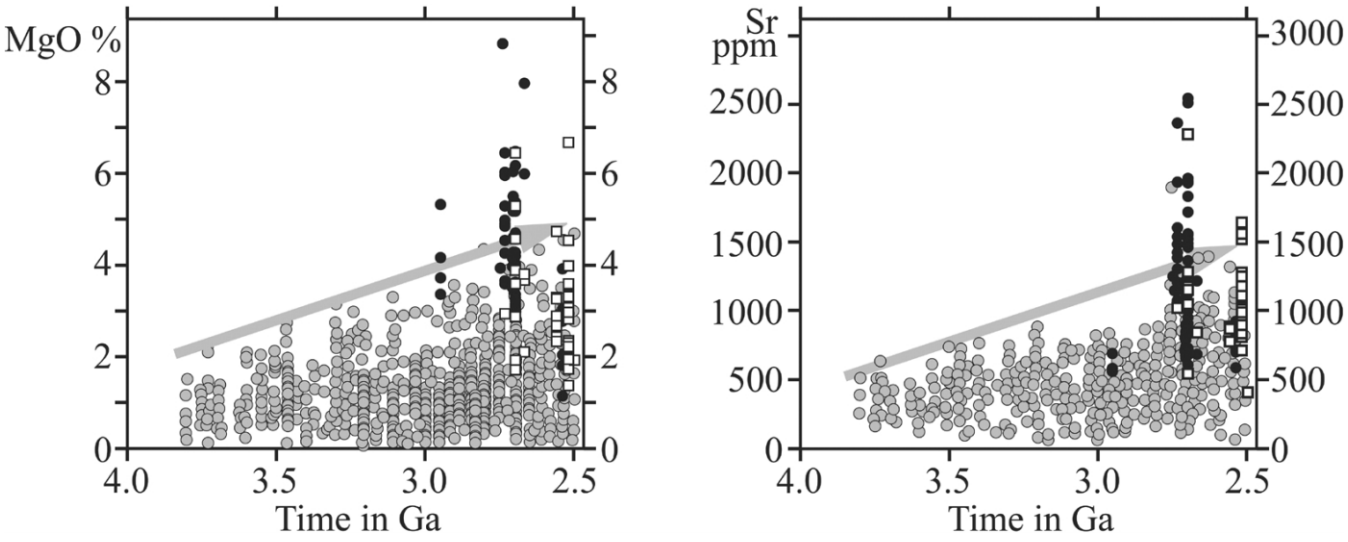

Figure 14 Diagrams showing the time-evolution of MgO and Sr content of the primitive TTG parental magmas (grey circles) from 4·0 Ga to 2·5 Ga (after Martin & Moyen 2002). The less different low-Ti (black circles) and high-Ti (open squares) sanukitoids have both MgO and Sr content far greater than in TTG, thus pointing to the fact that they were generated from a different source or/and a different mechanism.

However, most basalt melting experiments show that the amount of plagioclase stable together with garnet remains relatively low. Consequently, another possibility would be that in absence of significant amounts of residual plagioclase, Sr has an incompatible behaviour, its content in the magmatic liquid becoming only dependent on the degree of melting. In this case, the augmentation of Sr content in TTG magmas in the course of time would only reflect a decrease in the degree of melting of the basaltic source of TTG; which would also be consistent with the progressive cooling of the Earth. However, lower degrees of melting should result in lower Mg# and Ni and Cr contents in TTG magma, thus leading to an anti-correlation between Sr and Mg# (and Ni and Cr), whereas the opposite is observed. Whatever the cause of the time-dependent variation of Sr may be, it can be interpreted in terms of progressive cooling of the Earth, resulting in lower geothermal gradients in subduction systems (Fig. 13), thus leading to deeper slab melting. It must be noted that sanukitoids do not plot on this 'trend' but display significantly higher values for MgO and Sr (Fig. 14) as well as for Ni and Cr.

The present authors propose that throughout the Archaean, the Earth's heat production was high enough (curves 1 and 2, Fig. 13) to allow a high degree of melting of the subducted slab, consequently the 'effective melt:rock ratio' (as discussed above) was high and all slab melt was not consumed by mantle interaction, and was consequently emplaced largely as TTG. However, with time, Earth's geothermal gradient decreased and slab melting took place at progressively greater depths, such that some degree of interaction with peridotitic lithologies of the mantle wedge became increasingly likely. At about 2·7–2·5 Ga ago, further reduction in geothermal gradients resulted in smaller degrees of melting of the subducted slab, such that most of the TTG melts coming off the slab would be consumed in metasomatic reactions with peridotite. In these conditions, the mantle imprint would be stronger and could be achieved in two different ways: (1) in a single event where the mantle contamination and the generation of the sanukitoid melt are concomitant; this mechanism could result in low-Ti sanukitoid genesis; or (2) in a two-step process in which metasomatic minerals must crystallise in the mantle peridotite, before being destroyed by a subsequent melting event, thus giving rise to high-Ti sanukitoids (curve 3, Fig. 13). After Archaean times geothermal gradients were too low to allow slab melting and modern continental crust was generated by fluid metasomatised mantle wedge melting (curve 4, Fig. 13). This model accounts for the 'transitory' character of sanukitoids, as well as for their location at the Archaean–Proterozoic boundary.

4. Summary and conclusion

The temporal evolution of magmas at the Archaean–Proterozoic boundary can be synthesised as follows (Fig. 15):

1. In the Early Archaean (T>3·5 Ga), the terrestrial heat production was important, such that the subducted basalts underwent high degree of melting at shallow depth. The 'effective melt:rock ratio' in the mantle above the source of TTGs was high and the TTG magmas emplaced after minor or no interaction with the peridotite.
2. In the Middle to Late Archaean, the heat production was lower and the degree of melting of the subducted slab was slightly lower and took place at greater depth. However, the efficiency of slab-melting was high enough to maintain high slab-melt/mantle peridotite ratios. Thus, the slab-melt was not totally consumed in reaction with peridotite (Rapp *et al.* 1999, 2006), and consequently TTG magma was emplaced into the crust.
3. During the Late Archaean, and particularly at the Archaean–Proterozoic boundary, the Earth heat production and the efficiency of slab-melting had both declined. Slab-melt/mantle peridotite ratios had correspondingly declined such that slab-melts were almost totally consumed in reaction with mantle peridotite, thus producing Archaean sanukitoids. These later could result from either a single event where the mantle contamination and the generation of the sanukitoid melt are concomitant, (low-Ti sanukitoids) or from a two-step process where the mantle metasomatised by slab melts is subsequently molten (high-Ti sanukitoids).
4. Since the Lower Proterozoic, Earth's heat production was too low to allow subducted slab-melting under 'normal' conditions. Consequently, a slab dehydrates and classic BADR calc-alkaline magmatism results from melting of a peridotite that has been metasomatised by slab dehydration fluids.

https://doi.org/10.1017/S1755691009016120 Published online by Cambridge University Press

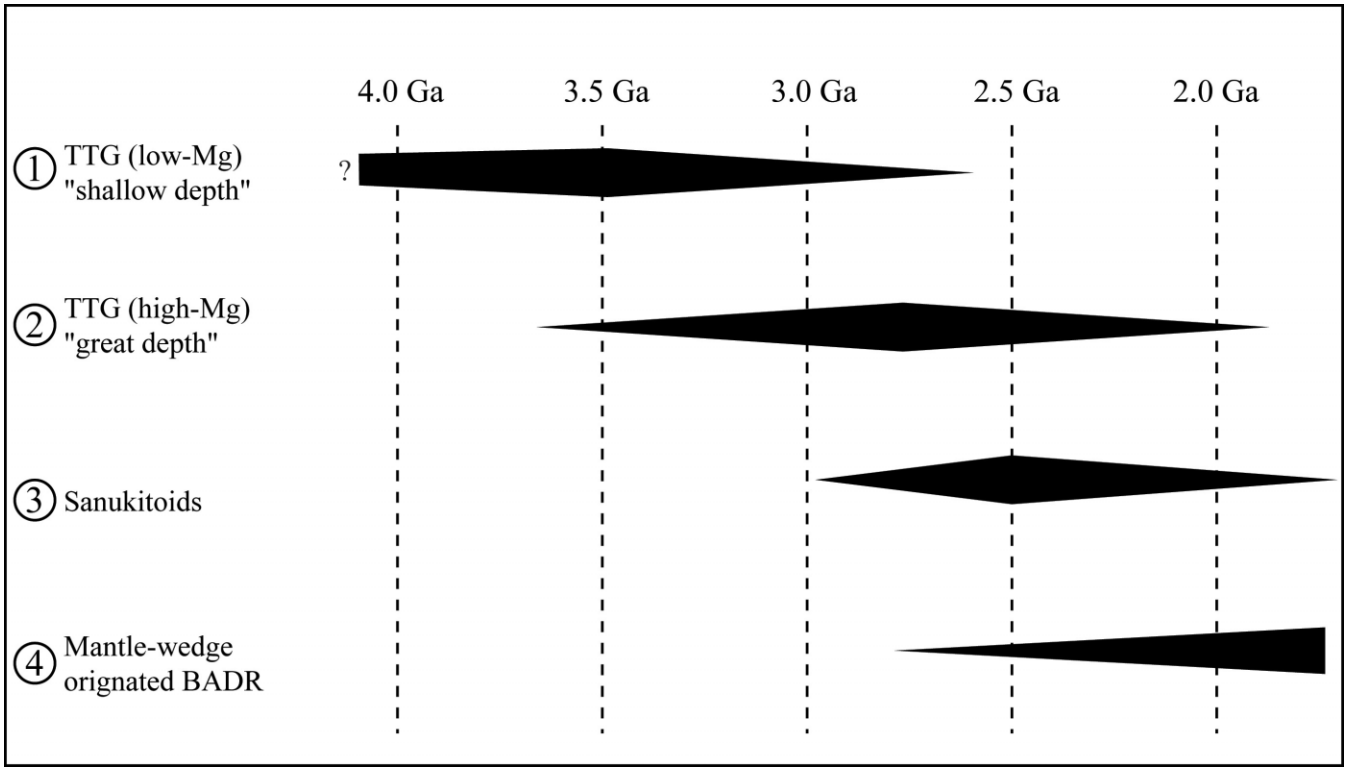

Figure 15 Schematic diagram illustrating the evolution of the juvenile crustal magmatism in course of the Earth's history. The thickness of the dark domain is qualitatively indicative of the volumetric importance of the magmatism. It clearly points to a large domain of overlapping at the Archaean–Proterozoic transition (2·5 Ga).

In other words, with regards to continental crust genesis, it appears that the Archaean–Proterozoic transition corresponds to a major change from a crustal (oceanic basalts) to a mantle source. The sanukitoid magmatism that shows both crustal and mantle imprint appears to be a good marker of these changes. Of course, this presentation of the timing of juvenile continental crust genesis over the course of Earth history is very simplistic and schematic. If today, in subduction environments, BADR magmatism is the more widespread, slab melting can also locally take place, leading to adakite genesis. Whenever, Archaean-like thermal regimes are established in the modern Earth, TTG-like (adakite) magmas are produced. However, this mechanism remains very minor on a global scale, but was once dominant. During Earth cooling, new thermodynamic conditions appeared, but not everywhere at the same time, because local conditions play an important role in controlling these thermodynamic regimes. This results in an overlap of petrogenetic mechanisms during time (Fig. 15), leading, for instance, to simultaneous TTG and sanukitoid magmatism: the apparently progressive character of petrogenetic changes near the Archaean–Proterozoic boundary is a statistic effect that reflects the progressive onset and development of some petrogenetic processes, and the diminishing importance of others. The dominant process of the Early Archaean was shallow slab melting that generated low-Mg TTG; this process became progressively less important during the later periods, and was all but replaced during Late Archaean times by deeper slab melting, which allowed for more significant interactions with mantle peridotite, and resulted in increased production of high-Mg TTG. Low-Mg TTG persisted late into the Archaean, even if not as important as they once were. In turn, the importance of high-Mg TTG decreased during the Proterozoic, and became a very rare process in the Phanerozoic; it was progressively replaced by BADR magmatic activity, which first appears in the Early Proterozoic and which became progressively dominant. Sanukitoids represent the 'missing link' between the (high-Mg) TTGs and the BADR; indeed, their transitional character is not only compositional but also chronologic, since they were emplaced about 2·5 Ga ago, during the transitional period between two epochs respectively dominated by TTG and BADR juvenile crustal magmatism.

5. References

Albarède, F. 1998. The growth of continental crust. *Tectonophysics* **296**, 1–14.

Althoff, F. J. 1996. *Etude pétrologique et structurale des granitoïdes de Marajoara (Pará, Brésil): leur rôle dans l'évolution archéenne du craton amazonien (2·7–3·2 Ga)*. Nancy: Henri Poincarré. 296 pp.

Arth, J. G. & Hanson, G. N. 1972. Quartz diorites derived by partial melting of eclogite or amphibolite at mantle depth. *Contributions to Mineralogy and Petrology* **37**, 164–74.

Atherton, M. P. & Petford, N. 1993. Generation of sodium-rich magmas from newly underplated basaltic crust. *Nature* **362**, 144–6.

Balakrishnan, S. & Rajamani, V. 1987. Geochemistry and petrogenesis of granitoids around Kolar schist belt: constraints for crustal evolution in Kolar area. *Journal of Geology* **95**, 219–40.

Barker, F. & Arth, J. G. 1976. Generation of trondhjemitic–tonalitic liquids and Archaean bimodal trondhjemite–basalt suites. *Geology* **4**, 596–600.

Barth, M. G., Foley, S. F. & Horn, I. 2002. Partial melting in Archaean subduction zones: constraints from experimentally determined trace element partition coefficients between eclogitic minerals and tonalitic melts under upper mantle conditions. *Precambrian Research* **113**, 323–40.

Barton, J. J. M., Doig, R., Smith, C. B., Bohlender, F. & van Reenen, D. D. 1992. Isotopic and REE characteristics of the intrusive charnoenderbite and enderbite geographically associated with the Matok Pluton, Limpopo Belt, southern Africa. *Precambrian Research* **55** (1–4), 451–67.

Bédard, J. 2006. A catalytic delamination-driven model for coupled genesis of Archaean crust and subcontinental lithospheric mantle. *Geochimica et Cosmochimica Acta* **70**, 747–71.

Bédard, P. 1996. Archean High-Mg monzodiorite plutonic suite: A reevaluation of the parental magma and differentiation. *Journal of Geology* **104**, 713–28.

https://doi.org/10.1017/S1755691009016120 Published online by Cambridge University Press

Blichert-Toft, J. & Albarède, F. 2008. Hafnium isotopes in Jack Hills zircons and the formation of the Hadean crust. *Earth and Planetary Science Letters* **265** (3–4), 686–702.

Bourdon, E., Eissen, J.-P., Gutscher, M.-A., Monzier, M., Hall, M. L. & Cotten, J. 2003. Magmatic response to early aseismic ridge subduction: the Ecuadorian margin case (South America). *Earth and Planetary Science Letters* **205** (3–4), 123–38.

Brown, G. C. 1985. Processes and problems in the continental lithosphère: geological history and physical implications. *In* Snelling, N. (ed.) *The chronology of the geological record. Geological Society, London, Memoir* **10**, 326–34. Bath, UK: The Geological Society Publishing House.

Calmus, T., Aguillon-Robles, A., Maury, R. C., Bellon, H., Benoit, M., Cotten, J., Bourgois, J. & Michaud, F. 2003. Spatial and temporal evolution of basalts and magnesian andesites ('bajaites') from Baja California, Mexico: the role of slab melts. *Lithos* **66** (1–2), 77–105.

Cavosie, A. J., Wilde, S. A., Liu, D., Weiblen, P. W. & Valley, J. W. 2004. Internal zoning and U–Th–Pb chemistry of Jack Hills detrital zircons: a mineral record of early Archean to Mesoproterozoic (4348–1576 Ma) magmatism. *Precambrian Research* **135** (4), 251–79.

Cavosie, A. J., Valley, J. W., Wilde, S. A. & E.I.M.F. 2005. Magmatic [delta]^{18}O in 4400–3900 Ma detrital zircons: A record of the alteration and recycling of crust in the Early Archean. *Earth and Planetary Science Letters* **235** (3–4), 663–81.

Cavosie, A. J., Valley, J. W. & Wilde, S. A. 2006. Correlated microanalysis of zircon: Trace element, [delta]^{18}O, and U–Th–Pb isotopic constraints on the igneous origin of complex >3900 Ma detrital grains. *Geochimica et Cosmochimica Acta* **70** (22), 5601–16.

Chardon, D., Peucat, J.-J., Jayananda, M., Choukroune, P. & Fanning, M. C. 2002. Archean granite-greenstone tectonics at Kolar (South India): Interplay of diapirism and bulk inhomogeneous contraction during juvenile magmatic accretion. *Tectonics* **21** (3), 7.1–7.17.

Condie, K. C. 1981. *Archaean greenstone belts.* Amsterdam: Elsevier. 434 pp.

Condie, K. C. 1989. *Plate tectonics and crustal evolution.* Oxford: Pergamon. 476 pp.

Condie, K. C. 2005. TTGs and adakites: are they both slab melts? *Lithos* **80**, 33–44.

Dalpé, C. & Baker, D. R. 2000. Experimental investigation of large-ion-lithophile-element-, high-field-strength-element- and rare-earth-element-partitioning between calcic amphibole and basaltic melt: the effects of pressure and oxygen fugacity. *Contributions to Mineralogy and Petrology* **140**, 233–50.

de Wit, M. J. 1998. On Archean granites, greenstones, cratons and tectonics: does the evidence demand a verdict? *Precambrian Research* **91** (1–2), 181–226.

Foley, S. F., Tiepolo, M. & Vannucci, R. 2002. Growth of early continental crust controlled by melting of amphibolite in subduction zones. *Nature* **417**, 637–40.

Forneris, J. F. & Holloway, J. R. 2003. Phase equilibria in subducting basaltic crust: implications for H_2O release from the slab. *Earth and Planetary Science Letters* **214**, 187–201.

Francis, D. & Ludden, J. 1995. The signature of amphibole in mafic alkaline lavas, a study in the Northern Canadian Cordillera. *Journal of Petrology* **36**, 1171–91.

Frost, C. D., Frost, B. R., Chamberlain, K. R. & Hulsebosch, T. P. 1998. The late Archaean history of the Wyoming province as recorded by granitic magmatism in the Wind River Range, Wyoming. *Precambrian Research* **89**, 145–73.

Glikson, A. Y. 1971. Primitive Archaean element distribution patterns: chemical evidence and geotectonic significance. *Earth and Planetary Science Letters* **12**, 309–20.

Grégoire, M., Jégo, S., Maury, R. C., Polvé, M., Payot, B., Tamayo, R. A. Jr. & Yumel, G. P. Jr. 2008. Metasomatic interactions between slab-derived melts and depleted mantle: Insights from xenoliths within Monglo adakite (Luzon arc, Philippines). *Lithos* **103** (3–4), 415–30.

Halla, J. 2005. Late Archean high-Mg granitoids (sanukitoids) in the southern Karelian domain, eastern Finland: Pb and Nd isotopic constraints on crust-mantle interactions. *Lithos* **79** (1–2), 161–78.

Harrison, T. M. & Schmitt, A. K. 2007. High sensitivity mapping of Ti distributions in Hadean zircons. *Earth and Planetary Science Letters* **261**(1–2), 9–19.

Hirose, K. 1997. Melting experiments on lherzolite KLB-1 under hydrous conditions and the generation of high-magnesian andesitic melts. *Geology* **25**, 42–4.

Hoffer, G. 2008. *Fusion partielle d'un manteau métasomatisé par un liquide adakitique: approches géochimique et expérimentale de la genèse et de l'évolution de l'arrière arc équatorien*. PhD Thesis, Université Blaise Pascal, Clermont Ferrand, France. 320 pp.

Jahn, B. M., Glikson, A. Y., Peucat, J.-J. & Hickman, A. H. 1981. REE geochemistry and isotopic data of Archaean silicic volcanics and granitoids from the Pilbara Block, western Australia: implications for the early crustal evolution. *Geochimica et Cosmochimica Acta* **45**, 1633–52.

Jahn, B.-M., Gruau, G., Capdevila, R., Cornichet, J., Nemchin, A., Pidgeon, R. & Rudnik, V. A. 1998. Archaean crustal evolution of the Aldan shield, Siberia: geochemical and isotopic constraints. *Precambrian Research* **91**, 333–63.

Jayananda, M., Martin, H., Peucat, J.-J. & Mahabaleswar, B. 1995. Late Archaean crust-mantle interactions in the Closepet granite, Southern India: evidence from Sr–Nd isotopes, major and trace element geochemistry. *Contributions to Mineralogy and Petrology* **119**, 314–29.

Johnson, A. D. & Wyllie, P. J. 1989. The system tonalite-peridotite-H_2O at 30 kbar, with applications to hybridization in subduction zone magmatism. *Contributions to Mineralogy and Petrology* **102**, 257–64.

Kamber, B. S., Ewart, A., Collerson, K. D., Bruce, M. C. & McDonald, G. A. 2002. Fluid-mobile trace element constraints on the role of slab melting and implications for Archaean crustal growth models. *Contributions to Mineralogy and Petrology* **144**, 38–56.

Käpyaho, A. 2006. Whole-rock geochemistry of some tonalite and high Mg/Fe gabbro, diorite, and granodiorite plutons (sanukitoid suites) in the Kuhmo district, eastern Finland. *Bulletin of the Geological Society of Finland* **78**, 121–41.

Kelemen, P. B., Shimizu, H. & Dunn, T. 1993. Relative depletion of niobium in some arc magmas and the continental crust: partitioning of K, Nb, La and Ce during melt/rock reaction in the upper mantle. *Earth and Planetary Science Letters* **120**, 111–34.

Kelemen, P. B., Hart, S. R. & Bernstein, S. 1998. Silica enrichment in the continental upper mantle via melt/rock reaction. *Earth and Planetary Science Letters* **164**, 387–406.

Kepezhinskas, P. K., Defant, M. J. & Drummond, M. S. 1996. Progressive enrichment of island arc mantle by melt-peridotite interaction inferred from Kamchatka xenoliths. *Geochimica et Cosmochimica Acta* **60**, 1217–29.

Kleinhanns, I. C., Kramers, J. D. & Kamber, B. S. 2003. Importance of water for Archaean granitoid petrology: a comparative study of TTG and potassic granitoids from Barberton Mountain and, South Africa. *Contributions to Mineralogy and Petrology* **145**, 377–89.

Kovalenko, A., Clemens, J. D. & Savatenkov, V. 2005. Petrogenetic constraints for the genesis of Archaean sanukitoid suites: geochemistry and isotopic evidence from Karelia, Baltic Shield. *Lithos* **79** (1–2), 147–60.

Kreissig, K., Holzer, L., Frei, R., Villa, I. M., Kramers, J. D., Kroner, A., Smit, C. A. & van Reemen, D. D. 2001. Geochronology of the Hout River Shear Zone and the metamorphism in the Southern Marginal Zone of the Limpopo belt, Southern Africa. *Precambrian Research* **109**, 145–73.

Krogstad, E. J., Hanson, G. N. & Rajamani, V. 1991. U–Pb ages of zircon and sphene for two gneiss terranes adjacent to the Kolar schist belt, South India: evidence for separate crustal evolution histories. *Journal of Geology* **99**, 801–16.

Krogstad, E. J., Hanson, G. N. & Rajamani, V. 1995. Sources of continental magmatism adjacent to late Archaean Kolar suture zone, south India: distinct isotopic and elemental signatures of two late Archaean magmatic series. *Contributions to Mineralogy and Petrology* **122**, 159–73.

Leite, A. A. S., Dall'Agnol, R., Macambira, M. J. B. & Althoff, F. J. 2004. Geologia e geocronologia dos granitóides arqueanos da região de Xinguara e suas implicações na evolução do Terreno Granito–Greenstone de Rio Maria, Cráton Amazônico. *Revista Brasileira de Geociencias* **34** (4), 447–58.

Liu, J., Bohlen, S. R. & Ernst, W. G. 1996. Stability of hydrous phases in subducting oceanic crust. *Earth and Planetary Science Letters* **143**, 167–71.

Lobach-Zhuchenko, S. B., Kovalenko, A. V., Krylov, I. N., Levskii, L. K. & Bogomolov, E. S. 2000. Geochemistry and petrology of the ancient Vygozero granitoids, Southern Karelia. *Geochemistry International* **38**, 584–99.

Lobach-Zhuchenko, S. B., Rollinson, H. R., Chekulaev, V. P., Arestovaa, N. A., Kovalenko, A. V., Ivanikov, V. V., Guseva, N. S., Sergeev, S. A., Matukov, D. I. & Jarvis, K. E. 2005. The Archaean sanukitoid series of the Baltic Shield: geological setting,

geochemical characteristics and implications for their origin. *Lithos* **79** (1–2), 107–28.

Lobach-Zhuchenko, S. B., Rollinson, H., Chekulaev, V. P., Savatenkov, V. M., Kovalenko, H., Martin, A. V., Guseva, N. S. & Arestova, N. A. 2008. Petrology of a Late Archaean, Highly Potassic, Sanukitoid Pluton from the Baltic Shield: Insights into Late Archaean Mantle Metasomatism. *Journal of Petrology* **49** (3), 393–420.

Macpherson, C. G., Dreher, S. T. & Thirlwall, M. F. 2006. Adakites without slab melting: High pressure differentiation of island arc magma, Mindanao, the Philippines. *Earth and Planetary Science Letters* **243** (3–4), 581–93.

Martin, E., Martin, H. & Sigmarsson, O. 2008. Could Iceland be a modern analogue for the Earth's early continental crust? *Terra Nova* **20**, 463–68.

Martin, E. & Sigmarsson, O. 2007. Low-pressure differentiation of tholeiitic lavas as recorded in segregation veins from Reykjanes (Iceland), Lanzarote (Canary Islands) and Masaya (Nicaragua). *Contributions to Mineralogy and Petrology* **154**, 559–73.

Martin, H. 1986. Effect of steeper Archean geothermal gradient on geochemistry of subduction-zone magmas. *Geology* **14,** 753–6.

Martin, H. 1987. Petrogenesis of Archaean trondhjemites, tonalites and granodiorites from eastern Finland: major and trace element geochemistry. *Journal of Petrology* **28**(5), 921–53.

Martin, H. 1993. The mechanisms of petrogenesis of the Archaean continental crust – comparison with modern processes. *Lithos* **30**, 373–88.

Martin, H. 1994. The Archean grey gneisses and the genesis of the continental crust. *In* Condie, K. C. (ed.) *The Archean crustal evolution. Developments in Precambrian Geology*, 205–59 Amsterdam: Elsevier.

Martin, H. 1999. The adakitic magmas: modern analogues of Archaean granitoids. *Lithos* **46**(3), 411–29.

Martin, H., Chauvel, C. & Jahn, B. M. 1983. Major and trace element geochemistry and crustal evolution of granodioritic Archaean rocks from eastern Finland. *Precambrian Research* **21**, 159–80.

Martin, H., Sabaté, P., Peucat, J.-J. and Cunha, J. C. 1997. Crustal evolution in the early Archaean of South America: example of the Sete Voltas Massif (Bahia State, Brazil). *Precambrian Research* **82**, 35–62.

Martin, H., Smithies, R. H., Rapp, R., Moyen, J.-F. & Champion, D. 2005. An overview of adakite, tonalite–trondhjemite–granodiorite (TTG), and sanukitoid: relationships and some implications for crustal evolution. *Lithos* **79** (1–2), 1–24.

Martin, H. & Moyen, J.-F. 2002. Secular changes in TTG composition as markers of the progressive cooling of the Earth. *Geology* **30**(4), 319–22.

Masuda, A., Nakamura, N. & Tanaka, T. 1973. Fine structures of mutually normalized rare-earth patterns of chondrites. *Geochimica et Cosmochimica Acta* **37**, 239–44.

Maury, R. C., Sajona, F. G., Pubellier, M., Bellon, H. & Defant, M. J. 1996. Fusion de la croûte océanique dans les zones de subduction/collision récentes: l'exemple de Mindanao (Philippines). *Bulletin de la Société Géologique de France* **167** (5), 579–95.

McGregor, V. R. 1979. Archaean grey gneisses and the origin of the continental crust: evidence the Godthaab region, west Greenland. *In* Barker, F. (ed.) *Trondhjemites, dacites and related rocks*, 169–204. Amsterdam: Elsevier.

Medeiros, H. & Dall'Agnol, R. 1988. Petrologia da porção leste do Batólito Granodiorítico Rio Maria, sudeste do Pará. *In Anais do 35 Congresso Brasileiro de Geologia*, 1488–99. Belém: Sociedade Brasileira de Geologia.

Millonig, L., Zeh, A., Gerdes, A. & Klemd, R. 2008. Neoarchaean high-grade metamorphism in the Central Zone of the Limpopo Belt (South Africa): Combined petrological and geochronological evidence from the Bulai pluton. *Lithos* **103** (3–4), 333–51.

Monzier, M., Robin, C., Hall, M. L., Cotton, J., Mothes, P., Eissen, J.-P. & Samaniego, P. 1997. Les adakites d'Equateur: modèle préliminaire. *Compte Rendus de l'Académie des Sciences de Paris* **324**, 545–52.

Moyen, J.-F. 2009. High Sr/Y and La/Yb ratios: the meaning of the 'adakitic signature'. *Lithos* **112**(3–4) 556–74.

Moyen, J.-F., Martin, H. & Jayananda, M. 1997. Origine du granite fini-Archéen de Closepet (Inde du Sud): apports de la modélisation géochimique du comportement des éléments en traces. *Compte Rendus de l'Académie des Sciences de Paris* **325**, 659–64.

Moyen, J.-F., Martin, H. & Jayananda, M. 2001a. Multi-element geochemical modelling of crust-mantle interactions during late-Archaean crustal growth: the Closepet granite (South India). *Precambrian Research* **112**, 87–105.

Moyen, J.-F., Nédélec, A., Martin, H. & Jayananda, M. 2001b. Contrasted granite emplacement modes within an oblique crustal section: the Closepet Granite, South India. *Physics and Chemistry of the Earth (A)* **26** (4–5), 295–301.

Moyen, J.-F., Martin, H., Jayananda, M. & Auvray, B. 2003. Late Archaean granites: a typology based on the Dharwar Craton (India). *Precambrian Research* **127** (1–3), 103–23.

Moyen, J.-F. & Stevens, G. 2006. Experimental constraints on TTG petrogenesis: implications for Archaean geodynamics. *In* Benn, K. Condie, K. C. & Mareschal, J. C. (eds) *Archaean geodynamics and environments. AGU Monograph* **164**, 149–75. Washington, DC: American Geophysical Union.

Nair, R. & Chacko, T. 2008. Role of oceanic plateaus in the initiation of subduction and origin of continental crust. *Geology* **36** (7), 583–6.

Nair, R. K. & Chacko, T. 2005. Oceanic plateaus: nuclei for Archean cratons. *Geological Society of America Annual Meeting, Salt Lake City*, 494. Boulder, Colorado and Lawrence, Kansas: The Geological Society of America and University of Kansas Press.

Nicholls, I. A. & Ringwood, A. E. 1973. Production of silica saturated tholeiitic magmas in island arcs. *Earth and Planetary Science Letters* **16**, 243–6.

Pawley, A. R. & Holloway, J. R. 1993. Water source for subduction zone volcanism: new experimental constrains. *Science* **121**, 664–7.

Prouteau, G., Scaillet, B., Pichavant, M. & Maury, R. C. 2001. Evidence for mantle metasomatism by hydrous silicic melts derived from subducted oceanic crust. *Nature* **410**, 197–200.

Querré, G. 1985. Palingenèse de la croûte continentale à l'Archéen: les graniteïdes tardifs (2·5–2·4 Ga) de Finlande orientale; pétrologie et géochimie. *Mémoires et Documents du Centre Armoricain d'Etude Structurale des Socles* **2.** Rennes: Université de Rennes.

Rapp, R. P., Watson, E. B. & Miller, C. F. 1991. Partial melting of amphibolite/eclogite and the origin of Archaean trondhjemites and tonalites. *Precambrian Research* **51**, 1–25.

Rapp, R. P., Shimizu, N., Norman, M. D. & Applegate, G. S. 1999. Reaction between slab-derived melts and peridotite in the mantle wedge: experimental constraints at 3·8 GPa. *Chemical Geology* **160**, 335–56.

Rapp, R. P., Shimizu, N. & Norman, M. D. 2003. Growth of early continental crust by partial melting of eclogite. *Nature* **425**, 605–9.

Rapp, R. P., Laporte, D., Martin, H. & Shimizu, N. 2006. Experimental insights into slab-mantle interactions in subduction zones: Melting of adakite-metasomatized peridotite and the origin of the 'arc signature'. *Geochimica et Cosmochimica Acta* **70** (18, Supplement 1), A517.

Rapp, R. P. & Watson, E. B. 1995. Dehydration melting of metabasalt at 8–32 kbar: implications for continental growth and crust-mantle recycling. *Journal of Petrology* **36** (4), 891–931.

Reddy, G. S. 1991. *Geochemistry and petrogenesis of granitic rocks around Sakarsanahalli (Kolar) South India.* PhD Thesis, Bangalore University, Bangalore. 147 pp.

Rogers, N. W. & Setterfield, T. N. 1994. Potassium and incompatible-element enrichment in shoshonitic lavas from the Tavua volcano. Fiji. *Chemical Geology* **118**, 43–62.

Rollinson, H. 1993. *Using geochemical data: evaluation, presentation, interpretation.* London: Longman. 352 pp.

Rollinson, H. 1997. Eclogite xenoliths in west African kimberlites as residues from Archaean granitoid crust formation. *Nature* **389**, 173–6.

Rudnick, R. L. 1995. Making continental crust. *Nature* **378**, 571–7.

Samsonov, A. V., Bogina, M. M., Bibikova, E. V., Petrova, A. Y. & Shchipansky, A. A. 2005. The relationship between adakitic, calc-alkaline volcanic rocks and TTGs: implications for the tectonic setting of the Karelian greenstone belts, Baltic Shield. *Lithos* **79** (1–2), 83–106.

Sarvothaman, H. 2001. Archaean High-Mg granitoids of mantle origin in the Eastern Dharwar craton of Andhra Pradesh. *Journal of the Geological Society of India* **58**, 261–8.

Schmidt, M. W. & Poli, S. 1998. Experimentally based water budgets for dehydrating slabs and consequences for arc magma generation. *Earth and Planetary Science Letters* **163** (1–4), 361–79.

Sekine, T. & Wyllie, P. J. 1982. The system granite-peridotite-H2O at 30 kbar, with applications to subduction zone magmatism. *Contributions to Mineralogy and Petrology* **81**, 190–202.

Sen, C. & Dunn, T. 1994. Experimental modal metasomatism of a spinel lherzolite and the production of amphibole-bearing peridotite. *Contributions to Mineralogy and Petrology* **119**, 422–32.

Shaw, D. M. 1970. Trace element fractionation during anatexis. *Geochimica et Cosmochimica Acta* **34**, 237–43.

Shirey, S. B. & Hanson, G. N. 1984. Mantle derived Archaean monzodiorites and trachyandesites. *Nature* **310**, 222–4.

Shirey, S. B. & Hanson, G. N. 1986. Mantle heterogeneity and crustal recycling in Archaean granite-greenstone belts: evidence from Nd isotopes and trace elements in the Rainy Lake province, Ontario, Canada. *Geochimica et Cosmochimica Acta* **50**, 2631–51.

Smithies, R. H. 2000. The Archaean tonalite–trondhjemite–granodiorite (TTG) series is not an analogue of Cenozoic adakite. *Earth and Planetary Science Letters* **182**, 115–25.

Smithies, R. H., Van Kranendonk, M. J. & Champion, D. C. 2005. It started with a plume – early Archaean basaltic proto-continental crust. *Earth and Planetary Science Letters* **238** (3–4), 284–97.

Smithies, R. H. & Champion, D. C. 1999. High-Mg diorite from the Archaean Pilbara Craton; anorogenic magmas derived from a subduction-modified mantle. *Geological Survey of Western Australia, Annual Review* **1998–99**, 45–59.

Smithies, R. H. & Champion, D. C. 2000. The Archaean high-Mg diorite suite: Links to Tonalite–Trondhjemite–Granodiorite magmatism and implications for early Archaean crustal growth. *Journal of Petrology* **41** (12), 1653–71.

Stern, R. 1989. *Petrogenesis of the Archaean sanukitoid suite*. New York: State University at Stony Brook. 275 pp.

Stern, R. A. & Hanson, G. N. 1991. Archaean high-Mg granodiorite: a derivative of Light Rare Earth enriched monzodiorite of mantle origin. *Journal of Petrology* **32**, 201–38.

Stevenson, R., Henry, P. & Gariépy, C. 1999. Assimilation-fractional crystallization origin of Archaean sanukitoid suites: Western Superior Province, Canada. *Precambrian Research* **96**, 83–99.

Sun, S. S. & McDonough, W. F. 1989. Chemical and isotopic systematics of oceanic basalts: implications for mantle composition and processes. *In* Saunders, S. D. & Norry, M. J. (eds) *Magmatism in the ocean basins. Geological Society, London, Special Publication* **42**, 313–45. Bath, UK: The Geological Society Publishing House.

Tatsumi, Y. 1989. Migration of fluid phase and genesis of basalt magma in subduction zones. *Journal of Geophysical Research* **94**, 4697–707.

Tatsumi, Y. & Ishizaka, K. 1982. Origin of high-magnesian andesites in the Setouchi volcanic belt, southwest Japan, I. Petrographical and chemical characteristics. *Earth and Planetary Science Letters* **60** (2), 293–304.

Viljoen, M. J. & Viljoen, R. P. 1969. The chemical evolution of the granitic rocks of the Barberton region. *Geological Society of South Africa Special Publication* **2**, 189–220.

Watson, E. B. & Harrison, T. M. 2005. Zircon thermometer reveals minimum melting conditions on earliest Earth. *Science* **308**, 841–4.

Wilde, S. A., Valley, J. W., Peck, W. H. & Graham, C. M. 2001. Evidence from detrital zircons for the existence of continental crust and oceans on the Earth 4·4 Ga ago. *Nature* **409**, 175–78.

Windley, B. F. & Bridgwater, D. 1971. The evolution of Archaean low- and high-grade terrains. *Geological Society of Australia Special Publication* **3**, 33–46.

Yaxley, G. M. & Green, D. H. 1998. Reactions between eclogite and peridotite: mantle refertilisation by subduction of oceanic crust. *Schweizeriche Mineralogische und Petrographische Mitteilungen* **78**, 243–55.

Zamora, D. 2000. *Fusion de la croûte océanique subductée: approche expérimentale et géochimique.* PhD Thesis, Université Blaise Pascal, Clermont-Ferrand, France. 314 pp.

MS received 1 February 2008. Accepted for publication 19 November 2008 (Stellenbosch); 15 January 2009 (RSE).